Studies of Canine Fibroblasts for Resources of Veterinary Regenerative Medicine

獣医再生医療の資源としての犬の線維芽細胞に関する研究

Joint Graduate School of Veterinary Medicine

Yamaguchi University

MELPA SUSANTI PURBA

March 2025

TABLE OF CONTENT

LIST OF TABLES

LIST OF FIGURES

ABSTRACT

Cell sheet technology has emerged as a promising approach for enhancing wound healing, particularly in challenging cases such as preventing postoperative complications. This method utilizes sheets of cells, which can promote tissue regeneration and accelerate the healing process through various mechanisms, including enhanced cell migration, angiogenesis, and cytokine secretion. Fibroblast is a well-known cell that produces cell sheets to improve wound healing. Fibroblasts play a crucial role in wound healing, acting as dynamic mediators of tissue repair through various mechanisms. Their functions include synthesizing extracellular matrix components, recruitment of immune cells, and modulation of inflammatory responses. When cell sheet technology shows great promise, challenges remain in standardizing production and ensuring consistent outcomes across different patient populations, especially in animals. The current studies established the cell sheet from canine fibroblast and investigated the effect of low-level laser therapy in canine fibroblast cells and fibroblast sheets.

The first chapter of the study is conducted to establish and characterize the canine multilayered fibroblast sheet from three origin tissues: oral mucosa, skin, and tail skin. Various methods have been developed to produce the cell sheet. This study uses large numbers of cells because this method is relatively simple and cost-effective compared with other cumbersome methods. A canine multilayered fibroblast sheet was produced using the large-numbers cell seeding method with Rho kinase inhibitor. Immunohistochemical examination revealed that the multilayered cell sheet comprised fibroblasts. Comparing the thickness of the cell sheet, the oral mucosa group showed the thickest layer compared to the others. In addition, we found that the proliferation of oral mucosal fibroblast was significantly higher than others, while the viability cell of the tree groups was more than 90%. The multilayered fibroblast sheets were successfully established from canine fibroblast.

The second chapter of the study describes the *in vivo* investigation, which was done by

autologously transplanting the oral mucosa fibroblast sheet into the canine's lobectomy. Histological evaluation showed thicker soft tissue with a thicker collagen deposit on the transplanted site than the control group (without transplantation). Transplantation of fibroblast sheets on canines may stimulate wound healing and prevent leakage postoperatively.

The third chapter of the study employs low-level laser (LLL) therapy to evaluate the effects of LLL irradiation in canine fibroblasts. LLL irradiation stimulates cell growth by regulating the expression of genes related to cell proliferation, cell migration, DNA synthesis, and others. Since our first study used large numbers to produce the sheet, an investigation of the proliferation of cells using LLL irradiation was done. In addition, the effect of LLL irradiation on migration cell ability and toxicity was evaluated along with proliferation cells. The investigation was done using an Erchonia® EVL dual-diode laser at wavelengths of 405 nm (5 mW) and 640 nm (7.5 mW) with irradiation times of 120, 360, and 1,800 sec. Our findings suggest that LLL therapy at wavelengths of 405 and 640 nm with an irradiation time of 120–360 sec (0.26–0.51 J/cm^2) can stimulate the proliferation and migration of canine fibroblasts without causing the toxicity effects. Besides the impact of LLL therapy stimulating the proliferation of cells, this finding may contribute to a better understanding of the beneficial role of LLL stimulation in canine wound healing.

The last chapter extends our investigation into the effect of LLL therapy in canine fibroblast sheets by examining the toxicity and thickness of the sheet. Since LLL irradiation can improve processes relevant to tissue regeneration, we evaluated whether LLL irradiation affects the formation of cell sheets. This study used an Erchonia® EVL dual-diode laser at wavelengths of 405 nm (5 mW) with energy densities of 0.17 and 0.51 J/cm^2 and 640 nm (7.5 mW) with energy densities of 0.26 and 0.77 J/cm^2. The irradiation was done for six different group treatments. LLL therapy influences the thickness of the fibroblast sheet, suggesting its potential to enhance the proliferation of cells. All the irradiation groups at each energy density

did not induce a higher cytotoxicity level than non-irradiation groups, demonstrating the safety of the LLL therapy. These findings suggest that LLL irradiation enhanced the thickness of the fibroblast sheet and was safely employed to produce the sheets.

In its entirety of chapters, the dissertation aims to provide primary data on regenerative medicine of canine fibroblast sheet combined with low-level laser therapy that stimulates wound healing. To the best of our knowledge, this is the first study to develop the canine fibroblast sheet and the first study to investigate the effect of LLL therapy on canine fibroblast cells and canine fibroblast sheet. The outcome of this research has considerable promise for improving regenerative medicine in the veterinary field.

GENERAL INTRODUCTION

Regenerative medicine promotes recovery from disease and injury by utilizing medical technology to repair, replace, or regenerate tissues or organs. As part of regenerative medicine, tissue engineering has been well-developed in human and animal models (rats and mice) to stimulate wound healing and prevent post-operative complications. The present study established multilayered fibroblast sheets from canines and investigated the effect of LLL therapy on canine fibroblast cells and fibroblast sheets.

Cell sheet therapy

Cell sheet engineering is an advanced tissue engineering technique in regenerative medicine focused on repairing or replacing damaged tissue and organs using various biological techniques (Thummarati *et al*., 2023). Various cell types, including mesenchymal stem cells, keratinocytes, and fibroblasts, fabricate cell sheets for wound treatment (Farabi *et al.,* 2024; Hu *et al*., 2023; Kirby *et al*., 2018; Li *et al*., 2019). These cell sheets can be detached as intact sheets and transplanted onto the wound site, where they promote the reattachment, migration, and proliferation of cells, leading to faster wound closure and reduced scarring (Benchaprathanphorn *et al*., 2020; Kim *et al*., 2023). Cell sheets synthesize and release essential cytokines and growth factors involved in wound healing, further enhancing tissue repair and regeneration (Ike *et al*., 2022; Matsuno *et al*., 2022; Mizoguchi *et al*., 2018; Nagase *et al*., 2020; Yoshimine *et al*., 2022). The cell sheet technology has potential clinical applications across various medical conditions (Chang *et al.*, 2023). They are beneficial in preventing postoperative complications (Fujino *et al*., 2023; Kim *et al*., 2018; Yoshimine *et al*., 2022). Cell sheets in animals showed effectiveness, including reinforcing the bronchial stump (Yoshimine *et al*., 2022), esophageal reconstruction (Yamamoto *et al*., 2023), regenerating mouse submandibular glands (Nam *et al*., 2019), preventing postoperative pancreatic fistula in rats (Iwamoto *et al*., 2021), and prevent perforation after duodenal endoscopic submucosal

dissection in a porcine model (Matsumoto *et al*., 2020). Thus, the transplantation cell sheets on the canine may enhance wound healing and address postoperative complications such as anastomotic leakage after esophagectomy or bronchopleural fistula.

Fibroblast

Fibroblasts play a crucial role in wound healing by contributing to tissue repair through various mechanisms. Fibroblasts produce extracellular matrix (ECM) components, promoting cell adhesion, tissue re-epithelialization, angiogenesis, and collagen formation (Cialdai *et al.,* 2022; Fernández-Guarino *et al.,* 2023; Gomes *et al.,* 2021; Plikus *et al.,* 2021). They are potential cells for regenerative medicine because they express high levels of intracellular fibroblast growth factors (Yanagihara *et al*., 2023), enhancing cell proliferation and migration (Kendall and Deghali-Bostwick, 2014; Smola *et al*., 1993; Trepat *et al*., 2012). Although not explicitly expressed on fibroblast, by using immunohistochemical evaluation, specific proteins, such as vimentin (VIM (protein), Vim (gene/mRNA mouse)) and fibroblast-specific protein 1 (FSP1, S100a4), have served as valuable markers to identify fibroblasts (Lendahl *et al*., 2022).

Low-level laser therapy

Low-level laser (LLL) therapy (also known as photobiomodulation) is a noninvasive treatment modality that uses low-power lasers with a specific wavelength of light to stimulate cellular processes without causing tissue heating, thereby promoting wound healing and reducing pain, enhancing ATP production and reducing oxidative stress (AlGhamdi *et al*., 2011; Avci *et al*., 2013; Dini *et al*., 2021; Kawasaki and Shimizu, 2000; Rola *et al*., 2022; Wickenheisser *et al*., 2019; Pedroni *et al*., 2018; Maghfour *et al*., 2024). LLL therapy has been applied for fibroblast biostimulation to improve wound healing (Gao and Xing, 2009; Gong *et al*., 2022; Lopez and Brundage, 2019; Shingyochi *et al*., 2017). Fibroblast proliferation and migration are essential parameters to enhance wound healing processes. Previous studies reported that applying LLL therapy in human and animal model cells increases cell

proliferation and migration (Peplow *et al*., 2010; Solmaz *et al*., 2017; Tam *et al*., 2020). LLL therapy has been practically reported to enhance wound healing in veterinary medicine. In dogs, Perego (2016) reported that LLL therapy resulted in significant differences in post-surgical wound healing and decreased the amount of exudates in the surgical area. LLL therapy also exhibited positive healing effects in canine osteoarthritis (Barale *et al*., 2020), skin disease (Perego *et al*., 2022), and chronic wounds (Hoisang *et al*., 2021).

A significant finding is the variability in LLL therapy application methods, including differences in laser type, dosage, and wavelength (Wickenheisser *et al*., 2019). LLL therapy is usually performed with visible or near-infrared laser light (390–1,100 nm) with relatively low fluences (0.04–50 J/cm^2) and power densities (<100 mW/cm^2) (AlGhamdi *et al*., 2011; Avci *et al*., 2013; Mussttaf *et al*., 2019; Peplow *et al*., 2010). The wavelength of visible light varies from 400 nm to 700 nm, which is divided by color, including violet/blue (400–500 nm), green (500–565 nm), yellow (565–590 nm), orange (590–625 nm), and red (625–700 nm) (Prado *et al*., 2023). Previous studies have shown the beneficial effects of LLL therapy on wound healing in humans and animals using violet/blue light (Etemadi *et al*., 2020; Masson-Meyers *et al*., 2016; Rossi *et al*., 2021) and red light (Crisan *et al*., 2013; Evans and Abrahamse, 2008; Kreisler *et al.*, 2003; Ma *et al.*, 2018; Moore *et al*., 2005; Schartinger *et al*., 2012; Taniguchi *et al*., 2019). These studies reported that LLL therapy stimulates cell proliferation and migration.

Cell sheet therapy– low-level laser therapy

Cell sheets are formed through self-assembly, allowing for high cell density and retention of extracellular matrix (ECM) components, which are crucial for tissue integration (Hu *et al*., 2023). Low-level laser therapy may improve cell processes relevant to tissue regeneration, such as survival, proliferation, migration, and differentiation. Moreover, LLL therapy can also prevent cell death and prolong cell longevity both *in vitro* and *in vivo*. LLL therapy and cell sheet technology improve processes relevant to tissue regeneration (Garrido

et al.,2019). By introducing fibroblast sheets and LLL therapy, the quality of treatment may be improved. To date, the information on the effect of LLL therapy in cell sheets is limited. Pedroni *et al*. (2018) reported that both technologies (cell sheet and LLL therapy) benefit tissue engineering and cell therapy that positively influences stem cell biology. A previous study reported that LLL therapy influences the composition and ultrastructure of the ECM of a cell sheet (Garrido *et al*., 2019). Therefore, LLL therapy may enhance the quality of cell sheet formation.

STUDY OBJECTIVE

Cell sheet technology is well developed as a regenerative medicine to repair tissue and prevent post-operative complications. To date, there are no reports on the production and therapeutic potential of the canine fibroblast sheet and limited information on the effect of low-level laser therapy on canine fibroblast cells and fibroblast sheets. Therefore, our first study aimed to investigate and establish the multilayered fibroblast sheets from canine fibroblast using oral mucosa, skin, and tail tissues. The second study investigated the effect of autologous fibroblast sheet transplantation in lobectomy canine models. The third study examined the effects of LLL irradiation at two different wavelengths (405 and 640 nm) and three different irradiation times (120, 360, and 1,800 sec) on canine fibroblast proliferation and wound closure. The last study aimed to investigate the effect of low-level laser irradiation on canine oral mucosal fibroblast sheets. Overall, we investigated the role of canine fibroblasts as a future regenerative medicine in the veterinary field.

CHAPTER I

Establishment and characterization of multilayered fibroblast cell sheets from the canine oral mucosa, skin, and tail

1.1 Abstract

Cell sheet therapy has been developed as an effective regenerative medicine to improve wound repair treatment and prevent postoperative complications. Fibroblasts are widely used to create cell sheet engineering because of their essential role in tissue regeneration and the acceleration of the wound healing process. The study aimed to establish the multilayered fibroblast sheets and assess the effect of autologous transplantation fibroblast sheets in canines. The study used fibroblasts from three origin canine tissues, including oral mucosa, skin, and tail skin. A canine fibroblast sheet was produced using the large-numbers cell seeding method with Rho kinase inhibitor. The assessment included viability cells, histological evaluation of the sheet, and secretion of vascular endothelial growth factor (VEGF) and monocyte chemoattractant protein-1 (MCP-1) of the fibroblast sheet. The three fibroblast groups successfully established a multilayered fibroblast sheet. Hematoxylin and eosin staining examination showed the thickest sheet in the oral mucosa fibroblast sheet. Immunohistochemical examination revealed that the multilayered cell sheet comprised fibroblasts expressed by vimentin. All multilayered fibroblast sheet groups secreted the VEGF and MCP-1. No differences were observed in the viability cells of each origin cell. The multilayered fibroblast sheets were successfully established from canine fibroblast. This finding provides the primary data for developing regenerative medicine in the veterinary field.

1.2 Introduction

Cell sheet therapy can be a promising method for promoting wound healing via tissue regeneration and accelerated wound healing process. Various cell types, including mesenchymal stem cells, keratinocytes, and fibroblasts, fabricate cell sheets for wound treatment (Farabi *et al*., 2024; Kirby *et al*., 2018; Li *et al*., 2019). These cell sheets can be detached as intact sheets and transplanted onto the wound site, where they promote the

reattachment, migration, and proliferation of cells, leading to faster wound closure and reduced scarring (Benchaprathanphorn *et al*., 2020; Kim *et al*., 2023). In addition, they can synthesize and release essential cytokines and growth factors involved in wound healing, further enhancing tissue repair and regeneration (Ike *et al*., 2022; Matsuno *et al*., 2022; Mizoguchi *et al*., 2018; Nagase *et al*., 2020; Yoshimine *et al*., 2022). Cell sheet transplantation is effective, i.e., cell sheets can be grafted to a target site to repair damaged tissues, including those in the articular cartilage, bone, periodontal ligaments, corneas, blood vessels, skin, and myocardium (Chen *et al*., 2015; Lee *et al*., 2019; Matsuno *et al*., 2022; Pakshir *et al*., 2020; Tsumanuma *et al*., 2016; Shirasaka *et al*., 2016). Further, they are beneficial in preventing postoperative complications (Fujino *et al*., 2023; Kim *et al*., 2018; Yoshimine *et al*., 2022). Thus, the transplantation cell sheets on the canine may enhance wound healing and address postoperative complications such as anastomotic leakage after esophagectomy or bronchopleural fistula.

Fibroblasts are involved in critical processes such as the breakdown of fibrin clots, angiogenesis, and the production of new extracellular matrix and collagen structures, which support other cells that are associated with effective wound healing and wound contraction (Bainbridge, 2013; Cialdai *et al*., 2022; Roman, 2023). Fibroblast sheets can have a significant potential in tissue engineering and wound healing (Benchaprathanphorn *et al*., 2020; Ike *et al*., 2022; Matsuno *et al*., 2022; Yoshimine *et al*., 2022). Fibroblast sheet therapy is widely developed using fibroblast from humans (Imamura *et al*., 2018; Kim *et al*., 2021; Matsushima *et al*., 2016), rats (Kanzaki *et al*., 2007; Yoshimine *et al*., 2022), and mice (Yamamoto *et al*., 2023; Ike *et al*., 2022; Matsuno *et al*., 2022) with various origin cells including skin, tail, and oral mucosa. Therefore, the canine fibroblast sheet was expected to have significant potential in treating various canine medical conditions.

Vascular endothelial growth factor (VEGF) is an important angiogenic factor that plays a significant role in angiogenesis (Ferrara, 2004; Johnson and Wilgus, 2014; Kendall and

Feghali-Bostwick, 2014). Monocyte chemoattractant protein-1 (MCP-1) chemokines mainly regulate the migration and infiltration of monocytes/macrophages (Deshmane *et al*., 2009). VEGF and MCP-1 were found in rats and mice fibroblast sheets, promoting wound healing (Nagase *et al*., 2020; Yoshimine *et al*., 2022; Ike *et al*., 2022).

Various methods to produce cell sheets already published include those cultured on a dish with thermo-responsive polymeric surfaces (Flores *et al*., 2008; Kanzaki *et al*., 2007; Nishimura *et al*., 2019) and those cultured using cell sheet engineering methods with thin biodegradable polymerized fibrin-coated dishes (Itabashi *et al*., 2005). A previous study (Yoshimine *et al*., 2022) developed multilayered fibroblast sheets by seeding large numbers of fibroblast. This cell sheet method is relatively simple and cost-effective compared with other cumbersome methods. Previous studies have reported *in vitro* and *in vivo* investigations in mice using multilayered cell sheets (Ike *et al*., 2022; Matsuno *et al*., 2022; Yoshimine *et al*., 2022). The multilayered cell sheets could be transplanted and engrafted more easily with favorable handling than monolayered cell sheets (Ike *et al*., 2022; Sakai *et al*., 2013).

Rho kinase (ROCK) inhibitors have shown beneficial effects in various cell cultures, including the promotion of cell aggregation by suppressing apoptosis (Watanabe *et al*., 2007; Gao *et al*., 2019), promotes cell adhesion (Gao *et al*., 2019), and cell attachment, migration, and proliferation (Croze *et al*., 2016; McGifford *et al*., 2022; Sun *et al*., 2015; Piltti *et al*., 2015). Matsumoto *et al*. (2022) reported that ROCK inhibitors inhibited the cell aggregate's collapse and formed the spherical cell aggregates. Studies in cell sheets are still unclear on whether ROCK inhibitors affect cell sheet formation.

To the best of our knowledge, there are no reports on the production and therapeutic potential of the canine fibroblast sheet. Therefore, this study aimed to investigate and establish the multilayered fibroblast sheets from canine fibroblast using oral mucosa, skin, and tail tissues with and without ROCK inhibitors. In addition, we evaluated the proliferation and

viability of the three canine fibroblast groups. The result of this study may provide essential data for developing regenerative medicine using fibroblast sheets in the veterinary field. We hypothesize that the fibroblast sheet can be produced using the oral mucosa, skin, and tail of canine fibroblasts.

1.3 Material and Methods

1.3.1 Animals

This study used four healthy beagles with a mean body weight of 13.79 ± 0.5 kg. The beagles' median age was 7.7 (range: 6.2–8.9) years. The dogs were housed in cages with free food and water access. The Ethics Committee of Animal Experiments of Yamaguchi University, Japan, approved this study (protocol number: 484).

1.3.2 Collection of tissue samples

Anesthesia was induced via the intravenous administration of propofol at a dose of 7 mg/kg (1% intravenous propofol; Pfizer Inc., Tokyo, Japan). An endotracheal tube was inserted into the trachea and connected to an anesthetic machine (Dräger Fabius® Plus, Lübeck, Germany). The anesthesia was maintained with isoflurane ((Mylan®, Pfizer, Tokyo, Japan) within a minimum alveolar concentration of 1.5–2. During anesthesia, Ringer's acetate solution at a flow rate of 5 mL/kg/hr (Veen F, Fuso Pharmaceutical Industries Ltd., Osaka, Japan) was administered intravenously to maintain the circulating blood volume. Subcutaneous carbazochrome sodium sulfonate at a dose of 0.5 mg/kg (Adna® Injection, Nipro ES Pharma Co., Ltd., Osaka, Japan) and intramuscular tranexamic acid at a dose of 10 mg/kg (Transamine®, Daiichi Sankyo Co., Ltd., Tokyo, Japan) were used as hemostatic agents. The analgesics used were intramuscular buprenorphine hydrochloride at a dose of 0.02 mg/kg (Lepetan®, Otsuka Pharmaceutical Co., Ltd., Tokyo, Japan) and intramuscular dexmedetomidine hydrochloride at a dose of 0.01 mg/kg (Dexdomitor®, Nippon Zenyaku

Kogyo Co., Ltd., Fukushima, Japan). The antibiotic is subcutaneous cefovecin sodium at 8 mg/kg (Convenia®, Zoetis Japan Co., Ltd., Tokyo, Japan). The oral mucosa, dorsal skin of the abdomen, and tail skin tissues of healthy beagle dogs were collected using a 6-mm biopsy trepan (Biopsy Punch, Kai Industries Co., Ltd., Gifu, Japan) with a tissue thickness of 3 mm.

1.3.3 Culture cells

The collected tissues were washed with phosphate-buffered saline (PBS) and penicillin/streptomycin (Fujifilm Wako Pure Chemical Industries, Ltd., Osaka, Japan) five times and then aseptically cut into 2-mm pieces or less with a Metzenbaum Scissor. The cells were isolated using 5,000 units of collagenase type I (Collagenase, Fuji Film Wako Pure Chemical Co., Ltd., Osaka, Japan) and cultured in DMEM medium (DMEM®, Life Technology Corporation, Grand Island, NY, USA) with 10% fetal bovine serum (Fetal Bovine Serum, Thermo Li Scientific Group, Tokyo, Japan), 100 U/mL penicillin, and 100 µg/mL streptomycin. The collagenase medium was filtered using a 70-µm cell strainer (FALCON®, Corning International Inc., Tokyo, Japan). After 8 hours, the cells were collected and seeded in the Dulbecco's Modified Eagle Medium (DMEM, 10% fetal bovine serum, and penicillin/streptomycin). The cells were cultured in an incubator for 3–5 days until fibroblast proliferation and adhesion were confirmed. After the cells were confirmed, the primary fibroblasts were seeded in a new DMEM medium with a cell density of 2.1×10^6 cells in an uncoated T-75 flask (FALCON®, Corning International Inc., Tokyo, Japan). Then, the cells were cultured until they occupied 70%–80% confluency.

1.3.4 Trypan blue exclusion assay

The trypan blue exclusion assay assessed the proliferation cell and viability in the second passage fibroblast. Initially, 1×10^5 cells/well for each cell were seeded in an uncoated six-well plate (FALCON®, Corning International Inc., Tokyo, Japan). For each fibroblast group, a series of five cultures were set up. One plate of the cells was collected every 24 h for 5 d, and the

cells were counted using a Burker Turk cytometer. Cell viability was calculated by dividing the viable cells by the total cell count and multiplying the ratio by 100.

$$Cell\ viability\ (\%) = \frac{total\ viable\ cells}{total\ cells} \times 100$$

1.3.5 Preparation of fibroblast cell sheets

For the cell sheet preparation method, this study referred to the multilayered sheet preparation method using rat-derived fibroblasts (Yoshimine *et al*., 2022). Fibroblasts at the second passage were used to produce the sheet. The cells were detached from the cell dish using TrypLE Express (TrypLE Express®, Life Technology Corporation, Grand Island, NY, USA). Primary fibroblast cells were seeded in a 24-well plate (5×10^5 cells/well) using a 2 mL medium consisting of DMEM and HFDM-1 (+) (Cell Science & Technology Institute, Miyagi, Japan) supplemented with 5% FBS. The ROCK inhibitor (Culture Sure® Y-27632, Fujifilm Wako Pure Chemical Industries, Ltd., Osaka, Japan) was evaluated by adding 2.5, 5, 10, 30, and 50 μM to the oral mucosa fibroblast culture. The surrounding wells without suspension cells were filled with 2 mL of the PBS to create uniform temperature around the suspension cells and cultured for 3 d at 37°C and 5% CO_2.

1.3.6 Enzyme-linked immunosorbent assay

The VEGF and MCP-1 concentrations were assessed using the supernatant fibroblast sheet after 3 days in the incubator. The enzyme-linked immunosorbent assay (ELISA) method following the manufacturer's instructions, VEGF (Canine VEGF, Funakoshi Co., Ltd., Osaka, Japan) and MCP-1 (Canine MCP-1, Funakoshi Co., Ltd., Osaka, Japan), and were measured using an Epoch spectrophotometer (BioTek, Winooski, VT, USA). All samples were assayed in triplicate.

1.3.7 Histological and immunohistochemical analyses

The prepared cell sheet was peeled off by pipetting and fixed with formalin. The fabricated cell sheets were placed on a raw ham to layer the sheet and embedded in paraffin.

Sections with a thickness of 3 μm were cut and mounted on the glass slides, deparaffinized in xylene, and rehydrated in a graded ethanol series (100%, 90%, and 70%). The glass slide was stained with hematoxylin and eosin (H&E). For immunostaining, heat-induced antigen retrieval was performed using the target retrieval solution with 10 times dilution (S1699; DakoCytomation A/S, Copenhagen, Denmark) at 95°C for 20 min, cooling for 20 min, and incubated with blocking buffer (X0909, DakoCytomation A/S, Copenhagen, Denmark) for 30 min at room temperature. The primary antibody was added and incubated for 60 min at room temperature. After washing, the secondary antibody was added and incubated for 60 min at room temperature. The primary and secondary antibodies were diluted with Dako anti-diluent with background. Immunostaining was performed using mouse monoclonal anti-vimentin antibody (1:500, ab8069, Abcam, Cambridge, UK) and secondary antibodies goat anti-mouse IgG (1:200, Alexa FluorTM488, A11029, Life Technologies, Waltham, MA, USA). The nuclei were stained using 4',6-diamidino-2-phenylindole dihydrochloride (DAPI) (PureBlu™ DAPI, Bio-Rad, Hercules, CA, USA) for 20 min at room temperature. All histological images were captured using a BZ-X710 microscope (Keyence, Osaka, Japan). The thickness of the fibroblast sheet based on H&E staining was measured using ImageJ (National Institutes of Health, Bethesda, MD, USA) in four parts randomly for four figures in each sheet.

1.3.8 Data analysis

Body weight was expressed as means ± standard deviations and age as median with range. The proliferation cell and viability of the fibroblast, ELISA results, and fibroblast sheet thickness were analyzed using a one-way analysis of variance, followed by the Tukey–Kramer HSD test for multiple comparisons test. These calculations were performed using the JMP software, version 9.0 (SAS Institute Japan, Tokyo, Japan). A P value of <0.05 was considered statistically significant.

1.4 Results

1.4.1 Morphological characteristics of fibroblast

Fig. 1.1 shows the morphological features of fibroblasts at the first passage from three origin tissues. The fibroblast had a spindle-shaped form. The three tissue groups did not show a difference in cell morphology.

1.4.2 Trypan blue exclusion assay

The oral mucosa fibroblast had the highest proliferation cells among the three tissue samples at all observation times (1–5 days). The proliferation cell of the fibroblast significantly differed between the oral mucosa group and the skin and tail skin groups ($P < 0.05$) (Fig. 1.2A). The cell viability of the three groups in all observation days was > 90% (Fig. 1.2B). The viability of the three cell groups did not significantly differ.

1.4.3 Canine fibroblast sheet

Using the following methods in rats, the cell sheet shrunk, the marginal sheet collapsed, and the sheet formation was difficult (Fig. 1.3). The ROCK inhibitor was evaluated in oral mucosa fibroblast to prevent shrinking fibroblast sheets. The results showed that adding 2.5 and 5 μM of ROCK inhibitor did not form a sheet while adding 10, 30, and 50 μM of ROCK inhibitor successfully made a sheet. Histological evaluation showed that the thickest layered sheet was established by adding 10 μM of ROCK inhibitor (Fig. 1.4). Therefore, 10 μM of ROCK inhibitor was added to each fibroblast group. A fibroblast sheet was produced (Fig. 1.5). Macroscopic observation of the oral mucosa fibroblast sheet showed circular shapes and was easy to detach from the 24-well plates. The tail fibroblast became a cell sheet, and the circular shape was maintained. Nevertheless, it was hard to detach from the culture plate. Meanwhile, the skin fibroblast became a cell sheet. However, its circular shape was not maintained and collapsed during detachment.

1.4.4 Enzyme-linked immunosorbent assay

The VEGF and MCP-1 concentrations were measured and summarized via graphs (Fig. 1.6). All fibroblast sheet groups secreted VEGF, and there were no significant differences between the three sheet groups. All groups produced MCP-1. The MCP-1 levels of the oral mucosa fibroblast significantly differed from the skin fibroblast. There were no significant differences between the oral mucosal group and the tail group.

1.4.5 Histological analysis of canine fibroblast sheets

Fig. 1.7 shows each sheet stained with H&E. All sheets are presented with multilayered cell sheets. The thickness values of the oral mucosa, skin, and tail fibroblast sheet were 40.10 ± 6.31, 19.44 ± 0.81, and 20.54 ± 3.47 μm, respectively (Fig. 1.8). The oral mucosa fibroblast sheet was thicker than the skin and tail fibroblast sheet. All fibroblast sheet groups tested positive for DAPI and vimentin (Fig. 1.9).

1.5 Discussion

In the current study, the canine multilayered fibroblast sheets were successfully established using fibroblast from the oral mucosa, skin, and tail skin by seeding large numbers of cells (Yoshimine *et al*., 2022) with ROCK inhibitor. VEGF and MCP-1 were secreted from the three fibroblast sheet groups, showing the potential of the sheet to stimulate healing processes. This study showed that the oral mucosa fibroblast tended to have a higher potential to create a favorable canine multilayered sheet than fibroblast from the skin and tail.

Fibroblasts are the most common cell type represented in connective tissues. The morphology of the cells remains the same even when it is present in multiple organ systems (Rinn *et al*., 2006). Regarding morphology, the fibroblasts are spindle-shaped with a centrally placed oval or round nucleus (Kalluri, 2016; Movat and Fernando, 1962; Ravikanth *et al*., 2011; Rinn *et al*., 2006). This study showed the fibroblasts from the three origins presented with a

spindle-shaped form under light microscope observation. No morphological differences were observed between the oral mucosa, skin, and tail groups.

The current study produced canine fibroblast sheets using the methods in rats (Yoshimine *et al*., 2022). On the first day of observation after seeding, the fibroblast did not retain its circular shape, and the margin of the sheet collapsed. This condition may occur due to the activity of myosin phosphorylation during sheet formation. Myosin phosphorylation regulated by ROCK plays an essential role in smooth muscle contraction and cell migration (Álvarez-Santos *et al*., 2020; Niggli, 1999; Matsumura *et al*., 2001; Seaholtz, 2003; Sun *et al*., 2020). Therefore, ROCK inhibitor was required to prevent smooth muscle contraction by suppressing the myosin phosphorylation activation (Kaneko-Kawano *et al*., 2012; Nakayama *et al*., 2005; Wirth, 2010; Yee *et al*., 2001). Previous studies on human nasal epithelial cell sheets have shown that ROCK inhibitors affect myosin regulation by inducing the downregulation of myosin light chain phosphorylation (Kasai *et al.*, 2020). Moreover, Okumura *et al.* (2017) have found that ROCK inhibitor enhances cell adhesion and engraftment by suppressing myosin phosphorylation in cultured corneal endothelial cell transplantation in primate models. In addition, several studies have reported that the inhibition of the ROCK signaling pathway significantly promotes cell aggregation, cell adhesion, and proliferation, suppresses T cell proliferation, and inhibits apoptosis/necrosis (Croze *et al*., 2016; Kim *et al*., 2022; Matsumoto *et al*., 2022; McGifford *et al*., 2022; Okumura *et al*., 2017; Peh *et al*., 2015). The current study successfully produced the multilayered canine fibroblast sheet from the oral mucosa, skin, and tail skin fibroblasts by adding 10 μM of ROCK inhibitor.

H&E staining was performed to evaluate the canine-layered cell sheets. Histological analysis showed that the oral mucosa, skin, and tail fibroblast sheet groups presented with multilayered cells. The oral mucosa fibroblast sheet was significantly thicker than the skin and tail skin fibroblast sheets. Immunohistochemistry staining showed that the oral mucosa, skin,

and tail fibroblast sheet groups tested positive for vimentin. Vimentin, which is a marker of fibroblast, is a type III intermediate filament protein that plays a role in wound healing progress, which is essential in promoting fibroblast proliferation, collagen accumulation, and epithelial-mesenchymal transition signals (Cheng *et al*., 2016; Coelho-Rato *et al*., 2024; Ridge *et al*., 2022). The presence of vimentin in all the fibroblast sheet groups indicated that applying a fibroblast sheet in the wound can promote fibroblast proliferation and stimulate wound healing.

VEGF is an endothelial cell-specific mitogen, an angiogenic inducer, and a vascular permeability mediator promoting neovascularization (Ferrara, 2004). Moreover, it contributes to endothelial cell migration, proliferation, and tube formation (Apte *et al*., 2019; Ferrara, 2004). MCP-1 is a member of the C-C family of chemokines, which is a potent chemotactic factor of monocytes that plays a vital role in wound healing processes by influencing inflammation, immune responses, tissue remodeling, fibroblast chemotaxis, and collagen synthesis (Arefieva *et al*., 2012; Deshmane *et al*., 2009; Yadav *et al*., 2010). A previous study showed that the proinflammatory MCP-1 promotes healing by restoring the macrophage response in mice with diabetic wounds (Wood, 2014). The current study showed that the three fibroblast sheet groups secreted VEGF and MCP-1. The VEGF result revealed that the oral mucosa and tail fibroblast sheet groups tended to be higher than the skin group. On the other hand, the oral mucosa groups showed a high tendency compared to other groups for MCP-1 assessment. The role of VEGF and MCP-1 was in accordance with the previous studies in mice and rats, which showed the fibroblast sheets produced various growth factors and cytokines including VEGF and MCP-1, which are essential in promoting the wound healing process (Ike *et al*., 2022; Matsuno *et al*., 2022; Mizoguchi *et al*., 2018; Nagase *et al*., 2020; Yoshimine *et al*., 2022).

Further, the current study used large numbers of fibroblasts to make the sheet. Cell proliferation and viability are considered when selecting the origin of fibroblasts. The trypan

blue exclusion assay is a standard method to assess cell viability by staining dead cells with compromised membranes, allowing the dye to enter while excluding the dye for live cells (Mani and Swargiary, 2023). In this study, the number of cell proliferation in the oral mucosa fibroblasts significantly increased compared with skin and tail fibroblasts. This result follows a previous study that showed human oral mucosa fibroblasts proliferated more than dermal fibroblasts (Lee and Eun, 1999). Previous studies have revealed that oral mucosa fibroblasts in mice exhibit a higher viability and promote faster healing with less scarring compared with dermal fibroblasts (Sezgin *et al*., 2021; Vijayashree and Sivapathasundharam, 2022). Interestingly, in this study, the cell viability of the oral mucosa, tail, and tail skin groups was >90%. Moreover, there was no significant difference between the three groups. Based on this result, the oral mucosa has a strong potential when it is used as a source of fibroblasts to develop canine regenerative medicine.

The current study had several limitations. First, the effect of ROCK inhibitor on myosin phosphorylation regulation, which can produce the canine fibroblast sheet, was not investigated. This is an important area for future research, as understanding the role of ROCK inhibitors in myosin phosphorylation regulation could enhance the efficiency of the fibroblast sheet production process. Second, various growth factors and cytokines were not examined, which are essential in promoting the wound healing process. Investigating these factors' role in fibroblast sheet production and wound healing could provide valuable insights for regenerative medicine. Finally, this study was performed regardless of age and sex in dogs. Hence, further studies should be performed to address these limitations and to explore the potential variations in the efficacy of the fibroblast sheet production process based on age and sex.

1.6 Conclusion

To the best of our knowledge, this is the first study to establish a method for creating a canine fibroblast sheet. In conclusion, we have successfully developed a method that can

produce a canine multilayered fibroblast sheet using large numbers of fibroblasts and ROCK inhibitors. Our results, which show that canine oral mucosa fibroblasts are superior to canine skin and tail fibroblasts, provide primary data for the use of canine fibroblasts in the development of regenerative medicine in the veterinary field.

Figures Chapter I

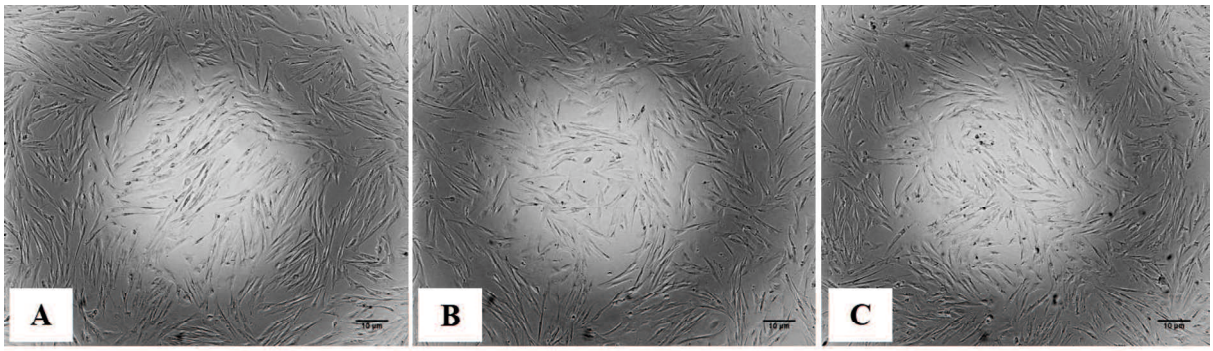

Figure 1. 1 Morphology of fibroblast. The canine fibroblast cells presented with a spindle-shaped single cell. (A) oral mucosa. (B) Tail skin. (C) Skin. Scale bars = 10 μm

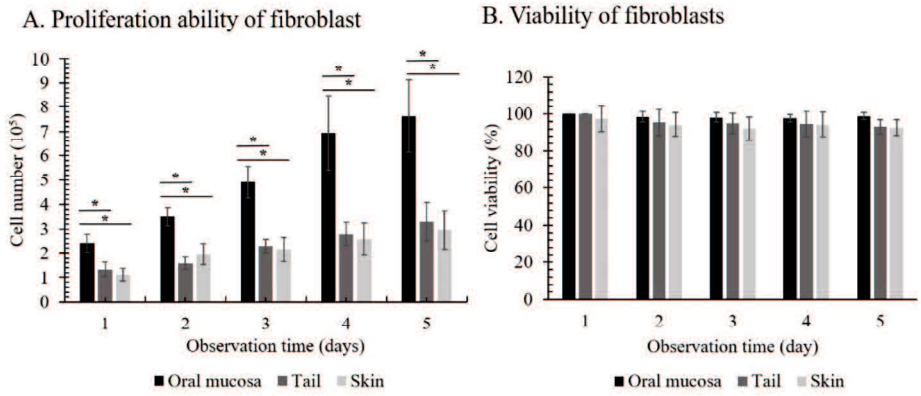

Figure 1. 2 The proliferation ability and viability of canine fibroblast cells. (A) The oral mucosa fibroblast cell had the highest proliferation ability. The proliferation ability significantly differed between the oral mucosa fibroblast cell group and the tail skin and skin fibroblast cell groups. (B) The cell viability of all groups was >90% during the 5-day observation. The cell viability did not vary significantly between the three groups. The fibroblast cells were counted every 24 hours during the 5-day observation. * $P < 0.05$

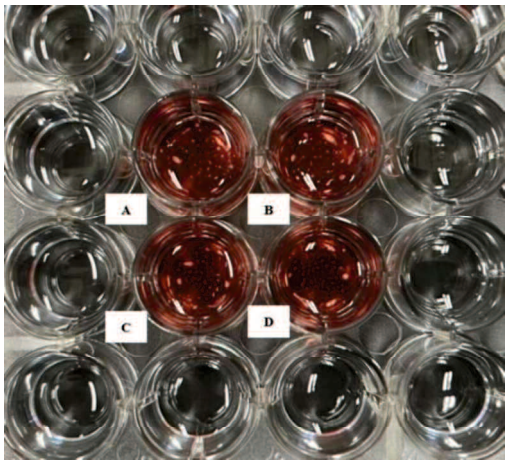

Figure 1. 3 Macroscopic image of the fibroblast sheet without ROCK inhibitor. The fibroblast sheet shrunk, and the margin collapsed. (A&B) Oral mucosa fibroblast sheet. (C) Skin fibroblast sheet. (D) Tail skin fibroblast sheet. The surrounding wells around the fibroblast sheets were filled with 2 mL of PBS to create a uniform temperature.

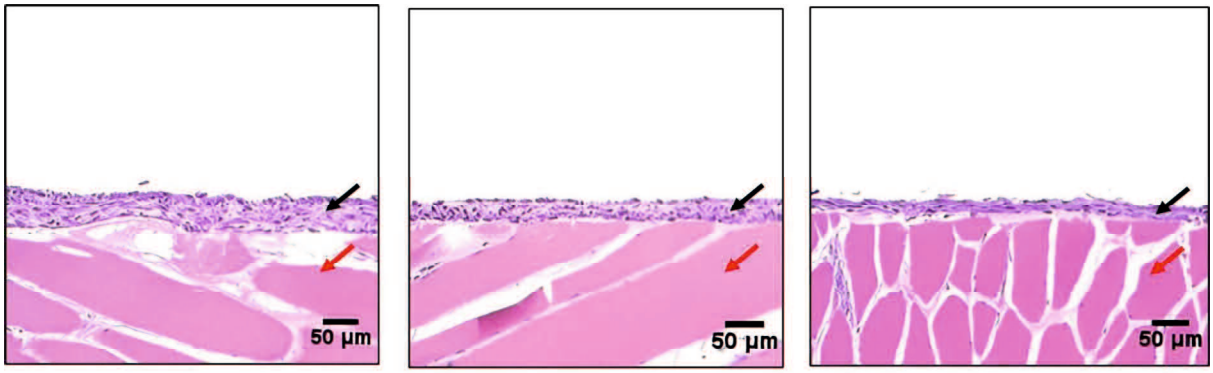

Figure 1. 4 H&E staining of the canine oral mucosa fibroblast sheets according to the amount of ROCK inhibitor (10, 30, and 50 μM). Histological staining was performed on the raw ham. Black arrow: a marker for the fibroblast sheet. Red arrow: a marker for the raw ham. Scale bars = 50 μm.

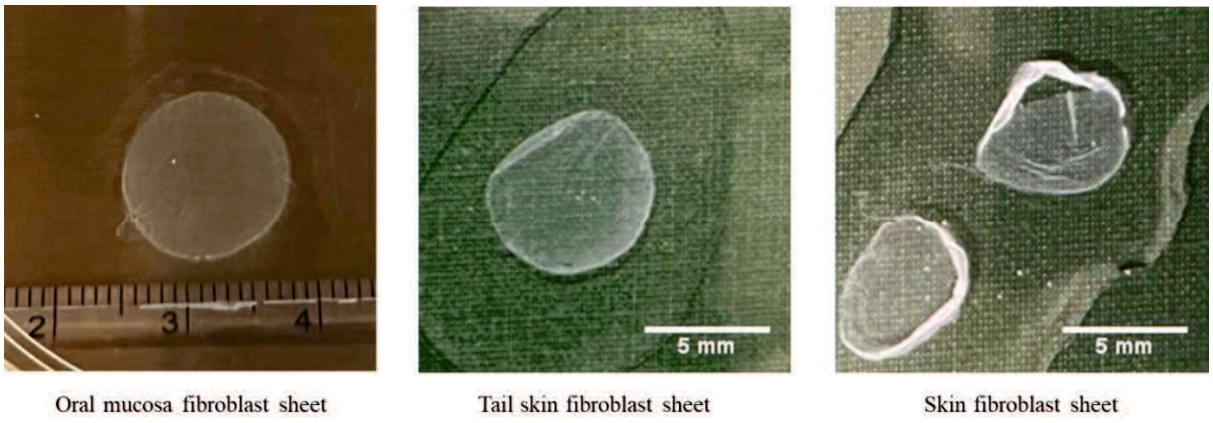

Figure 1. 5 Macroscopic image of the shape of the canine fibroblast sheet peeled from the dishes with Rho kinase inhibitor. Oral mucosa fibroblast sheet (left). Tail skin fibroblast sheet (middle). Skin fibroblast sheet (right). The skin fibroblast sheet did not retain its circular shape and collapsed during detachment. Scale bars = 5 mm.

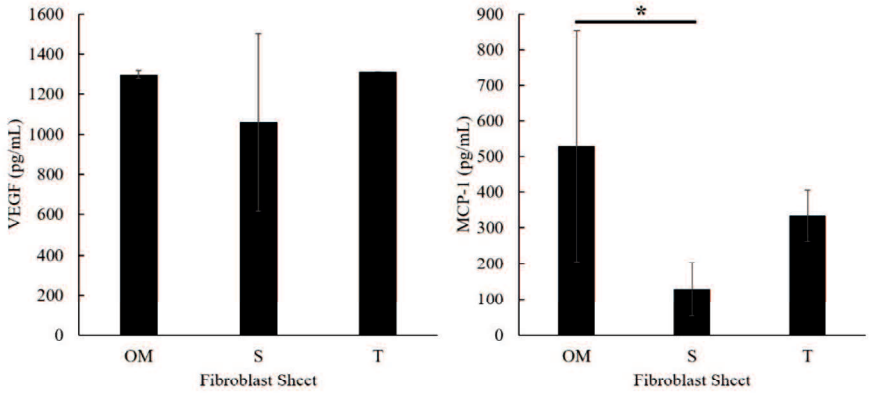

Figure 1. 6 VEGF (left) and MCP-1 (right) concentration in the culture supernatants of the canine fibroblast sheet that were cultured for 3 d (each bar, n = 4). All fibroblast sheet groups secreted VEGF and MCP-1. There were no significant VEGF values between the three groups. Significant differences in MCP-1 concentration were observed between oral mucosa and skin. OM: oral mucosa, S: skin, and T: tail skin. * $P < 0.05$

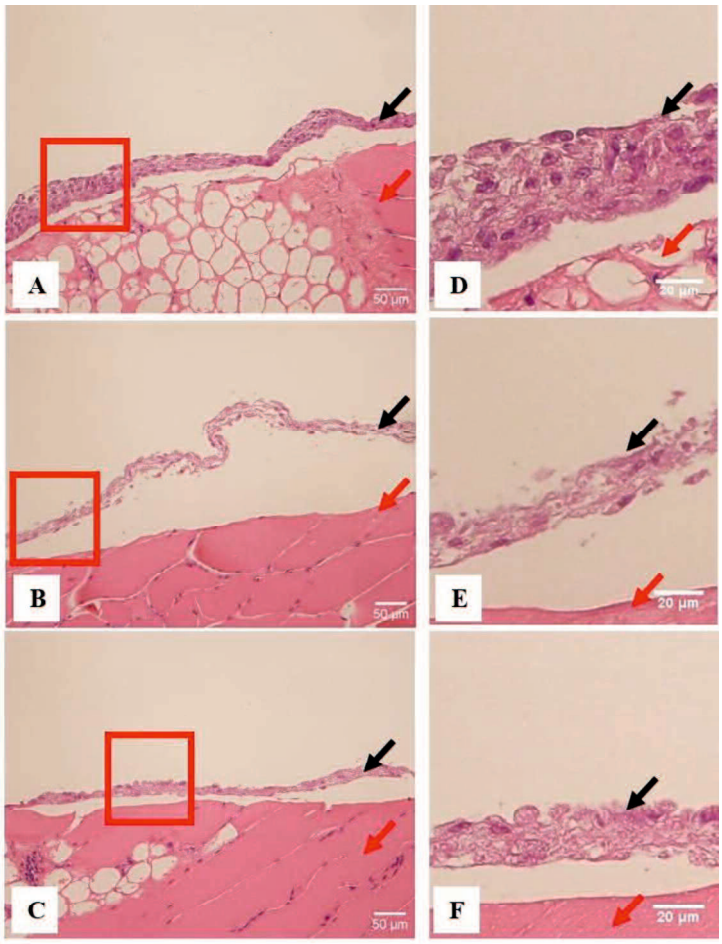

Figure 1. 7 H&E staining of the canine fibroblast sheets peeled from the dishes. Oral mucosa fibroblast sheet (A), skin fibroblast sheet (B), and tail skin fibroblast sheet (C). Observation at higher magnification of oral mucosa fibroblast sheet (D), skin fibroblast sheet (E), and tail skin fibroblast sheet (F). Histological staining was performed on the raw ham. Black arrow: a marker for the fibroblast sheet. Red arrow: a marker for the raw ham. Scale bars (A, B, C) = 50 µm. Scale bars (D, E, F) = 20µm

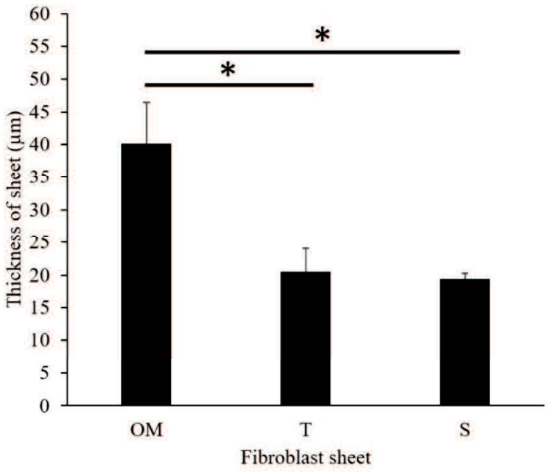

Figure 1. 8 The thickness of the canine fibroblast sheet according to the addition of 10 μM of Rho kinase inhibitor. The oral mucosa fibroblast cell had the thickest sheet. There were significant differences in thickness between the oral mucosa group and the skin and tail skin groups. OM: oral mucosa, S: skin, and T: tail skin. * $P < 0.05$.

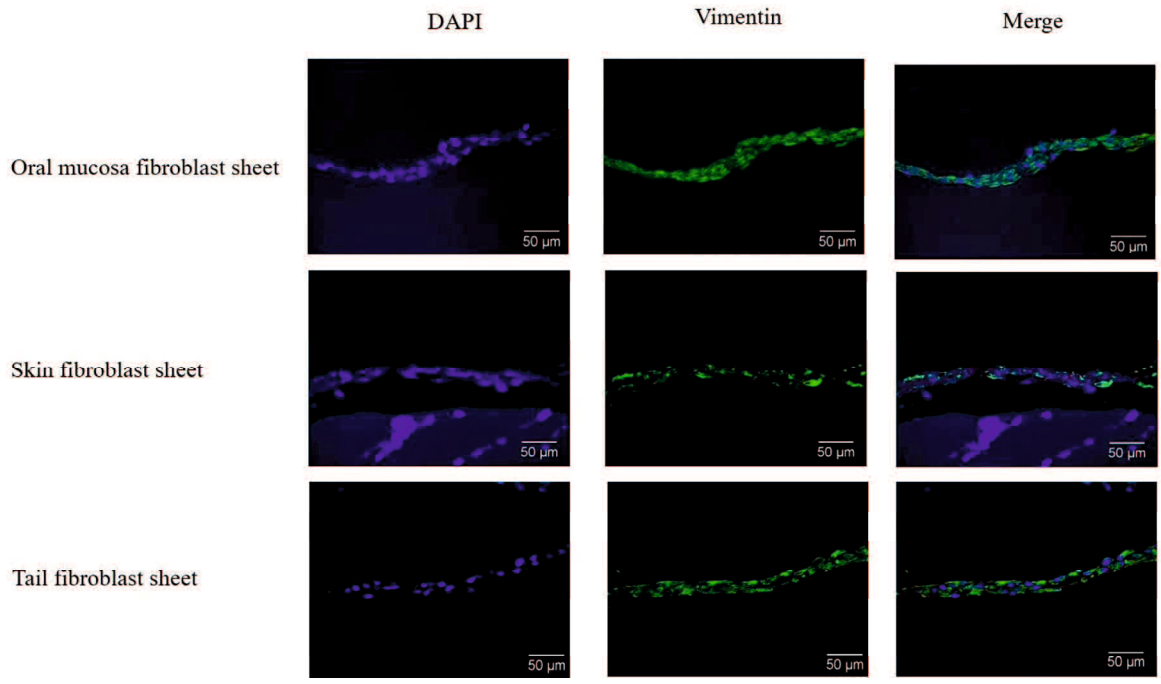

Figure 1. 9 Immunohistochemical fluorescence staining of the canine fibroblast sheets peeled from the dishes. Oral mucosa fibroblast sheet (upper), skin fibroblast sheet (middle), and tail skin fibroblast sheet (lower). All groups tested positive for DAPI and vimentin. Scale bars = 50 μm

CHAPTER II

Assessment of the effect of autologous fibroblast sheet transplantation in canine bronchial stump

2.1 Abstract

Bronchopleural fistula (BPF) is an abnormal connection between the bronchus and pleural cavity, associated with high morbidity and mortality. Fibroblasts play a critical role in wound healing by facilitating connective tissue formation, which was expected to prevent BPF. After lobectomy, the oral mucosal fibroblast sheet was transplanted autologously to the canine's bronchial stump. Histological evaluation, including hematoxylin-eosin and Azan staining, was performed seven days post-transplantation to evaluate the bronchial stumps. The autologous transplantation of fibroblast sheets formed connective tissue with collagen deposition, which is thicker than the nontransplantation groups. This promising result indicates that the fibroblast sheet stimulates wound healing and holds the potential to prevent leakage postoperatively for BPF.

2.2 Introduction

Bronchopleural fistula (BPF) is a critical complication associated with lung resection that is difficult to treat because a bronchial stump is incompletely healing (Endo *et al*., 2019; Imai *et al*., 2011). BPF can lead to further complications such as cause empyema, aspiration pneumonia, pneumothorax, and bronchopulmonary (Bof *et al*., 2007). BPF is rare in humans, occurring in 0.3% to 4.4% of resections, but it is characterized by high morbidity and mortality (Endo *et al*., 2019; Panagopoulos *et al.*, 2009). The mortality rate of BPF is estimated to be 12.5%-71.2% (Okuda *et al*., 2017; Tokunaga *et al*., 2020).

Even though there were no reports of the morbidity and mortality of BPF in dogs, some *in vivo* investigations were done on BPF in dogs (Makidono *et al*., 2020; Bof *et al*., 2007; Tao *et al*., 2006). Previous studies reported that the technique of bronchial stump closure is one of the principal factors responsible for the appearance of BPF, including manual suturing using absorbable sutures, ablation of bronchial mucosa with electric cautery and manual sutures,

stapling and reinforcement with manual sutures, or ablation and stapling followed by reinforcement with manual sutures (Murakami *et al*., 2016; Makidono *et al*., 2020; Bof *et al*., 2007; Arcerito *et al*., 1982). Although there are advantages to using those techniques, they are not totally free of complications. Currently, studies of cell transplantation on various organs have developed to prevent BPF. Previous studies reported that the local administration of bone marrow stromal cells (Gomez-de-Antonio *et al*., 2010), free fat tissue (Yoshimine *et al*., 2023), or adipose-derived stem cells (Llontop *et al*., 2014) effectively healed bronchial stumps in rat models.

As reported in Chapter 1, fibroblasts have a high potential as a cell source for fabricated cell sheets. As fibroblasts play a crucial role in wound healing, fibroblast sheet transplantation was expected to promote bronchial stump healing. Recently, a fibroblast sheet was reported to secrete growth factor in vitro and promoted angiogenesis, wound healing, and reinforced bronchial stump in a rat model (Yoshimine *et al*., 2022). This study, therefore, aims to evaluate the potential of autologous fibroblast sheet transplantation as a therapeutic or preventive method for BPF in dogs, a condition for which there are currently limited treatment options. We hypothesized that transplantation of multilayered fibroblast sheets can reinforce bronchial stumps in canine animal models.

2.3 Materials and Methods

2.3.1 Preparation of fibroblast cell sheets

For the cell sheet preparation method, this study referred to the multilayered sheet preparation method in Chapter 1. Briefly, fibroblasts at the second passage were used to produce the sheet. The cells were detached from the cell dish using TrypLE Express (TrypLE Express®, Life Technology Corporation, Grand Island, NY, USA). After centrifugation, the medium (DMEM + HFDM-1 (+) + 5% fetal bovine serum) was added to the cell suspension,

and the cell numbers were counted using a Burker Turk cytometer. A cell suspension (2.5×10^5 cells/mL) was prepared and dispensed 2 mL/well into an uncoated 24-well plate (FALCON®, Corning International Inc., Tokyo, Japan) and was added 10 μM of ROCK inhibitor (Culture Sure® Y-27632, Fujifilm Wako Pure Chemical Industries, Ltd., Osaka, Japan). The surrounding wells without suspension cells were filled with 2 mL of the PBS to create uniform temperature around the suspension cells and cultured for 3 days at 37°C and 5% CO_2.

2.3.2 Left pneumonectomy and transplantation of multilayered fibroblast sheets

This experiment was divided into control groups (without transplantation) and transplantation groups. A dog was fixed on the right recumbency position under general anesthesia. The thoracotomy was performed between the intercostal (fourth and fifth). A Finochet thoracotomy was applied to approach the left thoracic cavity. The left posterior lobe base was bluntly dissected to the main bronchus bifurcation, then the artery and vein pulmonary and bronchus were cut with a medical automatic cutting anastomosis device (Powered ECHELON FLEX® 7, PVE35A/Endoscopic Powered Linear Cutter 45, ECR45D, Johnson & Johnson Co., Ltd., Tokyo, Japan) and the left posterior lobe was excised (Fig. 2.1). The multilayered fibroblast sheets were transplanted to the bronchial closure suture. Immediately before transplantation, the medium was removed from the cell dish; the cell sheet was washed with PBS, and then 200 μl of fast green was added to stain the sheet for one minute. The fibroblast sheet was detached from the cell dish by pipetting. These procedures were performed aseptically. After closure, the bronchus was checked for leaks by flooding the chest cavity with physiological saline and applying a positive pressure breath up to 30 mmHg. After confirming no leakage, the intrathoracic cavity was washed with physiological saline. An intrathoracic drain was placed, and the thorax was closed according to the standard procedure.

2.4 Results

2.4.1 Left pneumonectomy and transplantation of multilayered fibroblast sheets

Both control and treatment groups underwent similar surgical procedures except for sheet implantation (Fig. 2.1). The average time of lobectomy is around four hours. There were no fatal operative errors during the operation. In the leak test, no leak was observed. Postoperatively, a chest tube was placed and managed for about one day. It was maintained until the pleural effusion was reduced and then removed. Complications from lobectomy to euthanasia included subcutaneous emphysema, pain, and decreased appetite, but no obvious respiratory complications. Macroscopic observation showed that the transplanted fibroblast disappeared within seven days postoperatively.

2.4.2 Histological analysis

Bronchial samples (Fig. 2.2) were stained with HE (Fig. 2.3) and Azan staining (Fig. 2.4). Compared to the control group, more tissue forms in the cell sheet group. Azan staining revealed collagen deposition within seven days after surgery in the fibroblast transplantation groups.

2.5 Discussion

This study used a pneumonectomy canine model to investigate the usefulness of the fibroblast sheet on the bronchial stump. Bronchopleural fistula (BPF) is a severe and potentially life-threatening condition characterized by an abnormal connection between the bronchi and the pleural cavity. The autologous transplantation of fibroblast sheets formed the connective tissue with collagen deposition, higher than in the control group, indicating that the fibroblast sheet stimulated wound healing and was expected to prevent leakage postoperatively.

In the present study, the effect of the transplanted sheets was evaluated using H&E and

Azan staining. Macroscopic observation showed that the transplanted fibroblast disappeared by seven days postoperatively. H&E staining showed more tissue formed in the excised bronchial wall of the transplantation groups than in the nontransplantation groups. These results indicate that the transplanted fibroblast may promote cell proliferation in the bronchial stump as a paracrine effect and result in tissue thickness. Azan staining confirmed that the transplantation groups had higher collagen deposition. Our results are in line with previous studies that reported that transplantation of fibroblast sheet might promote cell proliferation and contribute to increased collagen deposition, which is crucial for tissue strength and integrity in the transplanted area (Yoshimine *et al*., 2022; Ueno *et al*., 2016; Nagase *et al*., 2020; Yamamoto *et al*., 2023).

While a transplanted fibroblast sheet shows the potential to enhance the tissue thickness of the bronchial stumps post-operatively, it is essential to consider the evaluation of the myofibroblasts and vascularization, which are important for wound healing in bronchial stump post-sheet transplant. The initial time of the disappearing fibroblast sheet was unknown since this study only evaluated seven days post-transplantation. In addition, mechanical evaluation, such as burst pressure in the bronchial stump, is needed to strongly evaluate the fibroblast sheet's ability to reinforce the bronchial stump. Therefore, further studies should be performed to address these limitations.

2.6 Conclusion

To our knowledge, this represents the first study to evaluate the effect of autologous multilayered fibroblast sheets in canine models. The autologous transplantation of fibroblast sheets formed the connective tissue, including collagen deposition, higher than in the control group, indicating that the fibroblast sheet stimulates wound healing and prevents leakage postoperative. The usefulness of transplantation of refractory bronchial stumps may provide

options as a therapeutic or preventive method not only for current diseases but also for various diseases.

2.7 Figures Chapter II

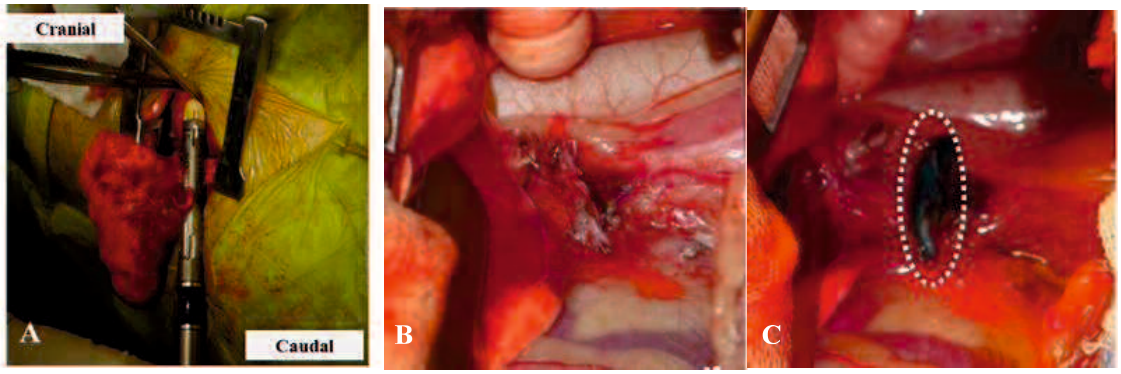

Figure 2. 1 Bronchial stump model. (A) The left posterior lobe was bluntly dissected to the main bronchus bifurcation and was cut with a medical automatic cutting anastomosis device (endoscopic powered linear cutter). (B) The left posterior lobe was excised. (C) The multilayered fibroblast sheet was transplanted to the bronchial closure suture. Dotted lines demarcate cell sheets.

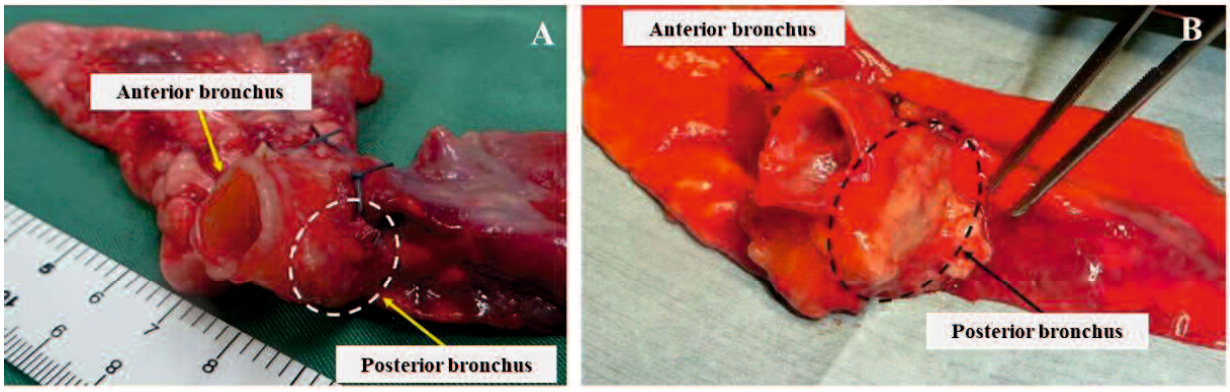

Figure 2. 2 Bronchial wound closure 1 week postoperative. The dotted white line is defined as wound closure in the nontransplantation group (A), and the dotted black line is defined as wound closure in the transplantation group (B)

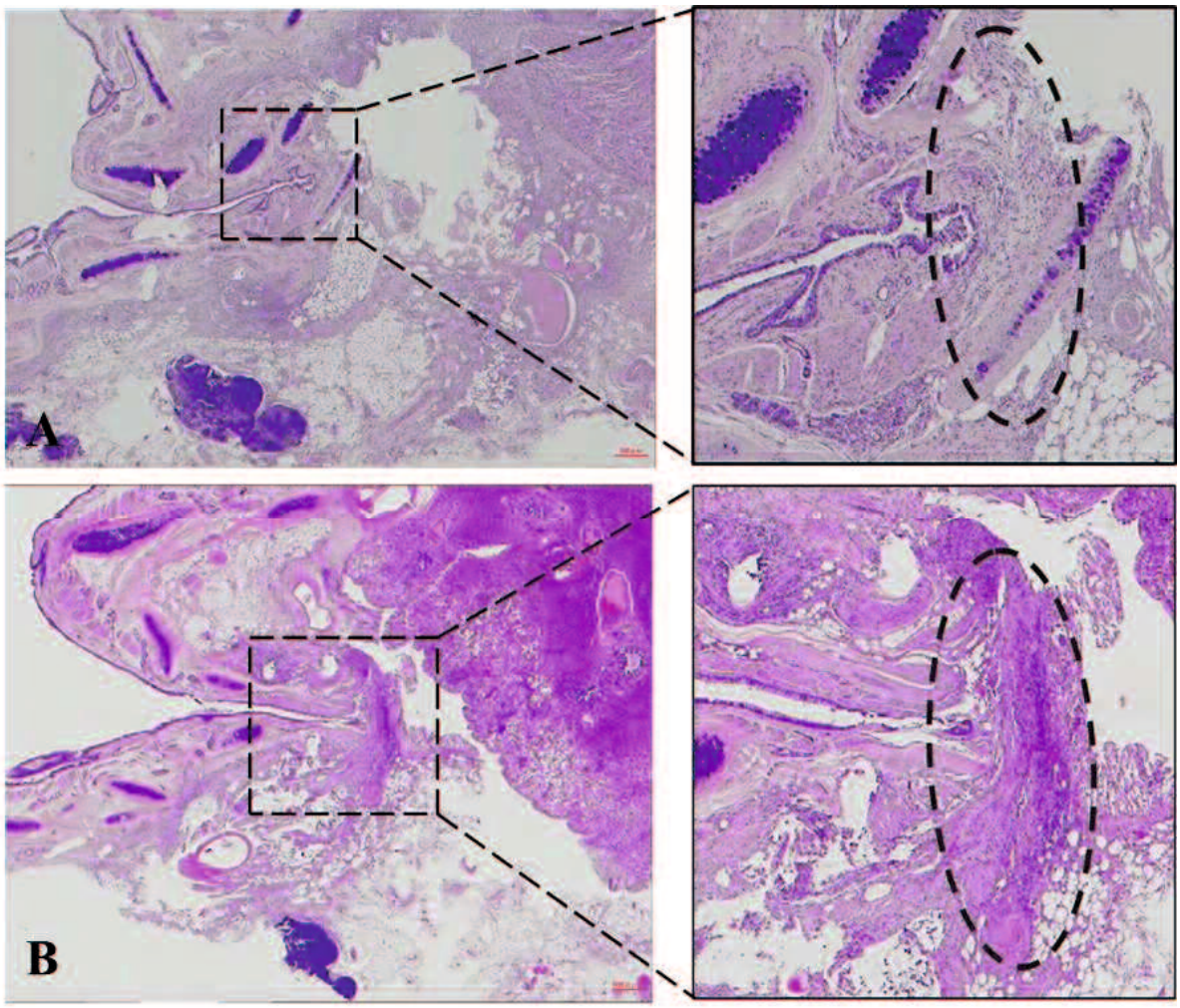

Figure 2. 3 Excised bronchial specimens were stained with H&E on day 7 postoperative. The bronchial wall of the membranous side was thicker in the fibroblast transplantation group than in the non-transplantation group (control). Control (A); Fibroblast transplantation (B). The black line is the defined area of the wound of the lobectomy. Scale bars: 500 μm.

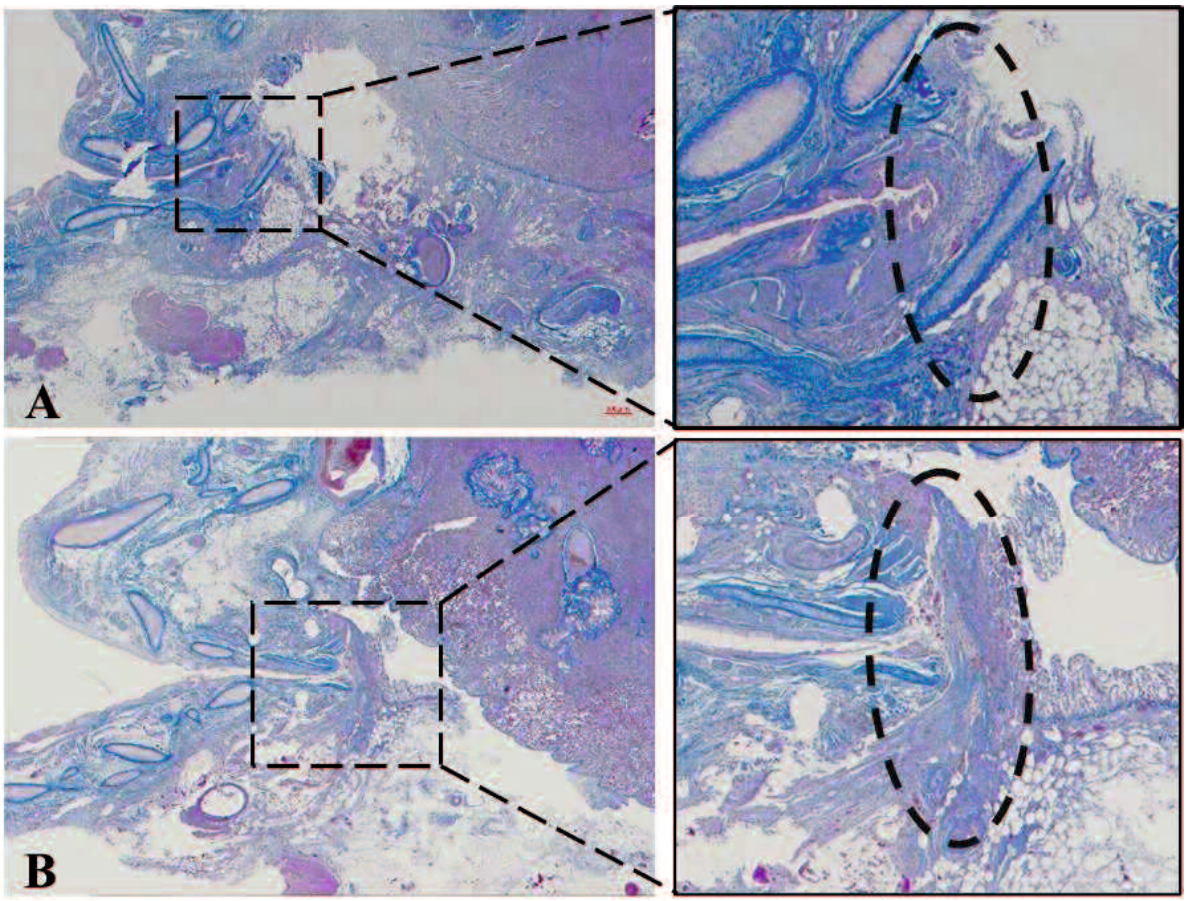

Figure 2. 4 Excised bronchial specimens were stained with Azan on postoperative day 7. Bronchial stumps of control individuals (top) and transplanted individuals (bottom). Dotted lines demarcate bronchial suture. Scale bars: 500 μm

CHAPTER III

Effects of low-level laser irradiation on canine fibroblasts

3.1 Abstract

Low-level laser (LLL) therapy is a well-known noninvasive treatment that stimulates fibroblasts to improve wound healing. LLL therapy can improve fibroblast proliferation and migration without causing toxicity. The present study aimed to evaluate the effects of two laser wavelengths at different irradiation times on canine fibroblasts. Fibroblasts were isolated from canine oral mucosa. After seeding for 24 hours, the fibroblasts were irradiated using the Erchonia® EVL dual-diode laser at wavelengths of 405 nm (5 mW) and 640 nm (7.5 mW) with irradiation times of 120, 360, and 1,800 sec. The proliferating and viability cells were evaluated 24 hours after laser irradiation. Wound closure rates were calculated at 0, 24, and 48 hours after laser irradiation. Parameters, including proliferation cell, cell viability, and cell migration, tended to be higher in the 360-sec group (405 nm) and 120-sec group (640 nm) than in other groups. Our findings suggest that LLL therapy at 405 and 640 nm wavelengths with an irradiation time of 120–360 sec (0.26–0.51 J/cm^2) can stimulate the proliferation and migration of canine fibroblasts. This finding may contribute to a better understanding of the beneficial role of LLL stimulation in canine wound healing.

3.2 Introduction

Fibroblasts play a crucial role in wound healing by contributing to tissue repair through various mechanisms. Fibroblasts produce extracellular matrix (ECM) components, promoting cell adhesion, tissue re-epithelialization, angiogenesis, and collagen formation (Cialdai *et al.,* 2022; Fernández-Guarino *et al.,* 2023; Gomes *et al.,* 2021; Plikus *et al.,* 2021). They are potential cells for regenerative medicine because they express high levels of intracellular fibroblast growth factors (Yanagihara *et al*., 2023), enhancing cell proliferation and migration (Kendall & Deghali-Bostwick, 2014; Smola *et al*., 1993; Trepat *et al*., 2012).

Low-level laser (LLL) therapy (also known as photobiomodulation) is a noninvasive

treatment modality that uses low-power lasers with a specific wavelength of light to stimulate cellular processes without causing tissue heating, thereby promoting wound healing and reducing pain in various in vitro and in vivo studies (AlGhamdi *et al*., 2011; Avci *et al*., 2013; Dini *et al*., 2021; Kawasaki &Shimizu, 2000; Rola *et al*., 2022). LLL therapy has been applied for fibroblast biostimulation to improve wound healing (Gao and Xing, 2009; Gong *et al*., 2022; Lopez and Brundage, 2019; Shingyochi *et al*., 2017). Fibroblast proliferation and migration are essential parameters to enhance wound healing processes. Previous studies reported that applying LLL therapy in human and animal model cells increases cell proliferation and migration (Peplow *et al*., 2010; Solmaz *et al*., 2017; Tam *et al*., 2020).

LLL therapy is usually performed with visible or near-infrared laser light (390–1,100 nm) with relatively low fluences (0.04–50 J/cm^2) and power densities (<100 mW/cm^2) (AlGhamdi *et al*., 2011; Avci *et al*., 2013; Mussttaf *et al*., 2019; Peplow *et al*., 2010). The wavelength of visible light varies from 400 nm to 700 nm, which is divided by color, including violet/blue (400–500 nm), green (500–565 nm), yellow (565–590 nm), orange (590–625 nm), and red (625–700 nm) (Prado *et al*., 2023). Previous studies have shown the beneficial effects of LLL therapy on wound healing in humans and animals using violet/blue light (Etemadi *et al*., 2020; Masson-Meyers *et al*., 2016; Rossi *et al*., 2021) and red light (Crisan *et al*., 2013; Evans and Abrahamse, 2008; Kreisler *et al.*, 2003; Ma *et al.*, 2018; Moore *et al*., 2005; Schartinger *et al*., 2012; Taniguchi *et al*., 2019). These studies reported that LLL therapy stimulates cell proliferation and migration.

LLL therapy has been practically reported to enhance wound healing in veterinary medicine. In dogs, Perego (2016) reported that LLL therapy resulted in significant differences in post-surgical wound healing and decreased the amount of exudates in the surgical area. LLL therapy also exhibited positive healing effects in canine osteoarthritis (Barale *et al*., 2020), skin disease (Perego *et al*., 2022), and chronic wounds (Hoisang *et al*., 2021). However, there is

limited information regarding the effects of LLL therapy on canine fibroblasts, which play a crucial role in wound healing processes. Therefore, the present study aimed to investigate the effects of LLL irradiation at two different wavelengths (405 and 640 nm) and three different irradiation times (120, 360, and 1,800 seconds) on canine fibroblast proliferation and wound closure. This study used primary oral mucosa fibroblast because it closely represents the origin tissue since the cells are taken directly from the tissue and not modified. Therefore, the results of this study are expected to be more representative of the tissues, which provide similar effects to in vivo and clinical conditions. We hypothesized that LLL therapy using 405 and 640 nm wavelengths can improve the proliferation and migration of canine oral mucosa fibroblasts. The results can provide data on canine fibroblasts to improve the application of LLL therapy in the veterinary field.

3.3 Material and Methods

3.3.1 Oral mucosa fibroblast cell culture

The protocol for collecting oral mucosa tissues was approved by the Committee on the Ethics of Animal Experiments of Yamaguchi University, Japan (Protocol Number 484). The oral mucosa tissues of three healthy beagles were collected independently using a 6-mm biopsy trepan (BIOPSY PUNCH, Kai Industries Co., Ltd., Gifu, Japan) with a thickness of tissue 3 mm. Fibroblast isolation was performed according to the previous studies (Adtani *et al*., 2019; mcLean and Pasumarthi, 2020; Yoshimine *et al*., 2022) following our first study. Briefly, the cells were isolated using 5,000 units of collagenase type I (Collagenase, Fujifilm Wako Pure Chemical Co., Ltd., Osaka, Japan) and cultured in Dulbecco's Modified Eagle Medium (DMEM®, Life Technologies Corporation, New York, NY, USA) with 10% fetal bovine serum (FBS, Thermo Fisher Scientific Group, Tokyo, Japan), and 100 U/mL penicillin and 100 µg/mL streptomycin (Penicillin-Streptomycin, Fujifilm Wako Pure Chemical Industries, Ltd., Osaka,

Japan). The oral mucosa tissues were incubated overnight at 37°C under 5% CO2 and then collected. The cells were cultured with DMEM medium in an incubator for 1 hour. Then, the medium was aspirated, and the new medium was added. Since healthy fibroblasts rapidly adhere to the flask, the adherent cells were defined as fibroblasts; this process removed the weakened fibroblast and other cells (such as mucosal epithelial cells). The cells were cultured for 3–5 days until fibroblast proliferation and adhesion were confirmed. Subsequently, primary fibroblasts were seeded in a new DMEM in an uncoated T-75 flask (FALCON®, Corning International Inc., Tokyo, Japan) and cultured until the cells were 70%–80% confluent. The second passage of fibroblasts was used in the experimental procedure.

3.3.2 Laser irradiation

LLL therapy was performed using the Erchonia® EVL dual-diode laser (Erchonia Corporation, Melbourne, FL, USA), which provides two laser diodes (405 nm [violet/blue laser beam] with an output of 5 mW and 640 nm [red laser beam] with an output of 7.5 mW). Each diode emits its wavelength with a tolerance of ±10 nm. Different groups were treated using two wavelengths (405 and 640 nm) with power output densities of 5 and 7.5 mW for 120, 360, and 1,800 seconds (Table 3.1). The irradiation time was determined within the range of previous reports (AlGhamdi *et al*., 2011; Huang *et al*., 2009; Moore *et al*., 2005; Peplow *et al*., 2010). The energy density (J/cm^2) for all treatment groups was calculated by multiplying the exposure time (seconds) by the laser's power output (W) divided by the surface area (cm^2). The surface area exposed to LLL therapy was identical to that of a 12-well plate (3.5 cm^2). The fibroblasts in the well plate without irradiation were treated similarly and used as a control. The laser's position was in contact with the bottom of the 12-well plate cover, with the laser beam placed at a 90° angle to the bottom of the 12-well plate, which was positioned in a stable supporting structure from Erchonia Corporation.

3.3.3 Lactate dehydrogenase (LDH) activity assay

The LDH enzyme was assessed using a commercially available kit for measuring LDH (Cytotoxicity LDH Assay Kit-WST, Dojindo Laboratories, Kumamoto, Japan). Canine oral mucosa fibroblasts were seeded in 12-well plates at an initial density of 1×10^5 cells/well and incubated for 12 hours. The laser irradiation protocol was performed as previously described (Table 3.1). The non-irradiated fibroblasts were used as a control group. After treatment for 24 hours, 100 μL of cell culture medium was transferred into a 96-well plate and added with 100 μL of LDH reaction solution, prepared according to the manufacturer's guidelines. The plate was covered with foil and incubated at room temperature for 30 minutes. Subsequently, 50 μL of stop solution was added, and the optical density of the solution was directly measured at 490 nm using an Epoch spectrophotometer (BioTek, Winooski, VT, USA). The LDH secretion data were presented as absorbance with optical density value. All experiments were performed thrice for repeatability.

3.3.4 Cell Counting Kit-8 (CCK-8) assay

Canine oral mucosa fibroblasts were seeded in 12-well plates at an initial density of 1×10^5 cells/well and incubated for 12 hours before exposure to laser irradiation. After irradiation, the cells were incubated for 24 hours. For the cell proliferation assay, 100 μL of cell culture medium and 10 μL of CCK-8 (Dojindo, Kumamoto, Japan) solution were added to each well. After incubation at 37°C for 2 hours, the optical density of the solution was measured at 450 nm using an Epoch spectrophotometer. The proliferation cell data were presented as absorbance with optical density value. The cell viability was shown as a percentage calculated according to the manufacturer's guidelines. The cell viability was calculated by dividing the average absorbance from each sample (sample-blank) by the control absorbance (control-blank) and multiplying by 100 (control: CCK-8 with medium and cells in a well [non-irradiated]; sample: CCK-8 with irradiated cells and medium; blank: CCK-8 and medium without cells in a well).

All experiments were performed thrice for repeatability.

3.3.5 Scratch wound healing assay

Scratch assay was performed to assess the effect of LLL irradiation on canine oral mucosa fibroblasts in response to injury. The canine oral mucosa fibroblasts were cultured in 12-well plates (2×10^5 cells/well) and incubated for 24 hours until a confluent monolayer of cells was confirmed. The scratch was performed across the cell layer with a 200-µL sterile pipet tip. The medium was removed, and the cells were washed with phosphate-buffered saline to remove debris. Then, 300 µL of DMEM was added, and irradiation was performed using LLL following the irradiation times (Table 3.1). After irradiation, 700 µL DMEM medium was added, and the cells were incubated. Photos were taken at 0, 24, and 48 hours after treatment via an inverted fluorescence microscope (Olympus, Tokyo, Japan) and analyzed using ImageJ software (National Institutes of Health, Bethesda, MD, USA). The wound closure rate was calculated by measuring the scratch area, which was not covered with fibroblast at 24 and 48 hours after treatment. The experiments were performed thrice for repeatability.

3.3.6 Statistical analysis

All data were represented as the mean ± standard deviation of three independent experiments. The data were analyzed using a one-way analysis of variance followed by the Tukey–Kramer honestly significant difference test (for multiple comparisons test). The calculations were performed using JMP software, version 9.0 (SAS Institute Japan, Tokyo, Japan). Statistical significance was considered at $P < 0.05$.

3.4 Results

3.4.1 Cell viability and LDH assay

The effects of LLL irradiation under different irradiation times on canine oral mucosa fibroblasts 24 hours after irradiation are shown in Fig. 3.1. The fibroblast proliferation and

viability tended to be higher in irradiated than in non-irradiated groups at both laser diode wavelengths. The highest proliferation of fibroblasts was observed in the 360-second group (0.51 J/cm^2) at a wavelength of 405 nm and in the 120-second group (0.26 J/cm^2) at a wavelength of 640 nm (Fig. 3.1A). Nevertheless, no significant differences were observed between the irradiated and non-irradiated groups at both wavelengths. The same results were also observed in terms of viability (Fig. 3.1B), wherein the highest viability was observed in the 360-second group at a wavelength of 405 nm and in the 120-second group at 640 nm. The viability of fibroblasts in the 120-second group at a wavelength of 640 nm significantly differed from that of other groups ($P < 0.05$). The results of the LDH cytotoxicity assay are shown in Fig. 3.2. No significant differences were observed in the LDH levels between the irradiated and non-irradiated groups ($P > 0.05$), with absorbance ranging from 0.375 to 0.391.

3.4.2 Scratch wound healing assay

The images of the scratch assay of both lasers (405 nm, Fig. 3.3) and (640 nm, Fig. 3.4) were acquired at 0, 24, and 48 hours after irradiation. At 24 and 48 hours, the irradiated fibroblasts at 405 and 640 nm wavelengths showed faster wound closure than non-irradiated cells (Fig. 3.5). At 24 and 48 hours, the 360-second group (0.51 J/cm^2) irradiated at a wavelength of 405 nm presented a rapid healing rate than other groups. Significant differences between irradiated (360 seconds) and non-irradiated fibroblasts were observed at 48 hours. Meanwhile, at 24 and 48 hours, a rapid healing rate was found in the 120-second group (0.26 J/cm^2) irradiated at a wavelength of 640 nm than in other groups. Statistical differences were observed between the non-irradiated and irradiated groups (120 and 360 seconds) at 24 hours. Meanwhile, at 48 hours, significant differences were observed between the irradiated (120-second) and non-irradiated groups.

3.5 Discussion

In the present study, we evaluated the effects of irradiation using two laser wavelengths on the cell viability and migration of canine oral mucosa fibroblasts. In both laser wavelengths (405 and 640 nm) at different irradiation times (120, 360, and 1,800 sec), the fibroblast viability and migration tended to be higher compared with the control group (0 sec). All the treatment groups did not induce a higher cytotoxicity level than the control group. This finding indicates that laser therapy under these conditions stimulates the proliferation and migration of oral mucosa fibroblasts, is not harmful, and might be safely employed for irradiation of canine oral mucosa fibroblasts.

LDH assay assessed cell damage by releasing the cytosolic glycolytic enzyme LDH into the medium due to plasma membrane permeabilization after irradiation (Kabakov and Gabai, 2018). No statistically significant difference in LDH concentration was observed between the non-irradiated and irradiated groups, indicating that both laser wavelengths and their fluences were not harmful to living fibroblasts. This result is in line with a previous study (Hou *et al*., 2008), where LLL irradiation did not show a significant difference in LDH levels between the non-irradiated and irradiated groups.

Fibroblast viability and migration were investigated in vitro to evaluate the effects of two laser wavelengths on canine oral mucosa fibroblasts. Fibroblast viability was evaluated by assessing dehydrogenase activity in living cells. CCK-8 (also known as WST-8 assay) has been widely used to assess cell viability and cytotoxicity by detecting high NAD(P)H levels using tetrazolium salt, which directly corresponds to dehydrogenase activity and provides a measure of cellular metabolic activity (Chamchoy *et al*., 2019; Fan *et al*., 2024). A scratch assay was performed to evaluate and compare cell migration. Scratch assay (wound healing assay) is a technique to evaluate cell migration in vitro by scratching a confluent cell monolayer to create a new artificial gap and observing the movement of cells in the scratch area (Grada *et al*., 2017;

Liang *et al*., 2007; Rodriguez *et al*., 2005). Cell migration is fundamental in various biological phenomena, including tissue homeostasis, wound healing, and immune response (Cialdai *et al*., 2022; Trepat *et al*., 2012). Fibroblasts migrate and proliferate into the wound site and are required to produce and secrete proteases from the ECM to heal the wound site (Kendall and Deghali-Bostwick *et al*., 2014; Trepat *et al*., 2012).

In the present study, the proliferation, viability, and migration of fibroblasts tended to be higher in all irradiated groups than in the non-irradiated groups, which was expected. This finding indicates that the laser with a 405 and 640 nm wavelength and a specific fluence rate could promote fibroblast proliferation and migration, both essential in normal wound healing processes. Fibroblasts that were irradiated for 360 sec at a wavelength of 405 nm showed higher proliferation and viability; however, no significant differences were observed compared with other groups. In contrast, fibroblasts that were irradiated for 120 sec at a wavelength of 640 nm showed higher proliferation and viability; however, no significant differences were observed compared with other groups. Wound closure was faster in the irradiated groups than in the non-irradiated groups. The groups irradiated for 360 sec at 405 nm and for 120 sec at 640 nm showed more rapid wound closure than other irradiated groups. This finding indicates that using the Erchonia® EVL dual-diode laser in one-time irradiation for 120–360 sec at a fluence of 0.2–0.5 J/cm^2 stimulates canine oral mucosa fibroblast proliferation and wound closure. This result is in line with previous in vitro studies using human fibroblasts at a wavelength of 640 nm (Hawkins and Abrahamse, 2007; Smola *et al*., 1993) and animal models (Gong *et al*., 2022; Solmaz *et al*., 2017), which reported the advantages of LLL therapy in wound healing, including cell proliferation and migration. Prado *et al*. (2023) performed a scoping review of the effects of photobiomodulation with blue light (400–500 nm) on wound healing. They summarized that blue light at a low energy density (<20 J/cm^2) stimulates different cell types and proteins, but blue light at a high energy density (20.6–50 J/cm^2) reduces cell proliferation, migration, and

metabolism. Studies on human dermal fibroblasts reported that using blue light at a wavelength of 470 nm with an energy density of 5 J/cm^2 (Masson-Meyers *et al*., 2016) and 420 nm with an energy density of 3.43 J/cm^2 (Rossi *et al*., 2021) stimulated cell proliferation. Etemadi *et al*. (2020) also reported that LLL therapy with blue diode laser at power densities of 400 mW/cm^2 with irradiation times of 10 and 15 sec corresponding to energy densities of 4 and 6 J/cm^2 exerted statistically significant positive effects on the proliferation and migration of gingival fibroblasts. These findings suggest that combining blue and red light stimulates fibroblast proliferation and migration.

Overall, among the irradiated groups, the group that was irradiated for 1,800-second (2.5–3.9 J/cm^2) at wavelengths of 405 and 640 nm showed the slowest proliferation and wound closure rate, suggesting that the time and dose of irradiation are essential to the cell response. Huang *et al*. (2009; 2011) summarized the biphasic dose responses in LLL therapy on culture cells in vitro, animal models in vivo, and clinical studies. Based on the three-dimensional model of the Arndt–Schulz curve, they suggest that too much power density and/or time may lead to the inhibition effect of LLL therapy. Another study reported that using a wavelength of 632.8 nm at high doses (10 and 16 J/cm^2) increased cellular damage and decreased cellular viability and proliferation in human skin fibroblasts (Hawkins and Abrahamse, 2007). Similarly, Flores Luna *et al.* (2020) proved the principle of the Arndt–Schulz law, wherein small doses provide positive stimuli to the cellular environment, and higher doses cause deleterious effects, inhibiting cellular activity. They found a significant reduction in the number of cells using 3.61 and 3.16 J/cm^2 of energy compared with 0.45 and 0.75 J/cm^2 of energy at 660 nm. The concept of biphasic dose–response is essential in LLL therapy because of the large number of illumination parameters for each treatment and laser characteristic (AlGhamdi *et al*., 2011; Avci *et al*., 2013; Huang *et al*., 2009; Huang *et al*., 2011).

To date, the exact mechanism of LLL therapy in influencing cellular processes is not yet

well established and is likely multifactorial. Studies reported that LLL therapy interacts with mitochondrial chromophores (Greco *et al*., 1989; Hamblin, 2018; Karu *et al*., 2005), modulates reactive oxygen species that increase energy production (adenosine triphosphate), and stimulates enzymes and transcription factors (Avci *et al*., 2013; Chung *et al*., 2011; Hamblin, 2018; Pavlov *et al*., 2024; Rola *et al*., 2022) that improve wound healing. Therefore, further studies should investigate these factors in canine oral mucosa fibroblasts.

3.6 Conclusion

To the best of our knowledge, this is the first study that uses canine oral mucosa fibroblasts to investigate the effects of LLL irradiation in vitro on the wound healing process, especially cellular proliferation, and migration. We concluded that the Erchonia® EVL dual-diode laser with two wavelengths (405 and 640 nm) has a stimulating effect on the proliferation and migration of canine fibroblasts with an irradiation time of 120–360 sec without causing cytotoxicity. This finding may contribute to a better understanding of the beneficial role of LLL stimulation in wound healing in canines.

3.7 Table Chapter III

Table 3. 1 The energy density of different groups

Laser diode	120 seconds	360 seconds	1,800 seconds
405 nm	0.17 J/cm^2	0.51 J/cm^2	2.57 J/cm^2
640 nm	0.26 J/cm^2	0.77 J/cm^2	3.86/cm^2

3.8 Figures Chapter III

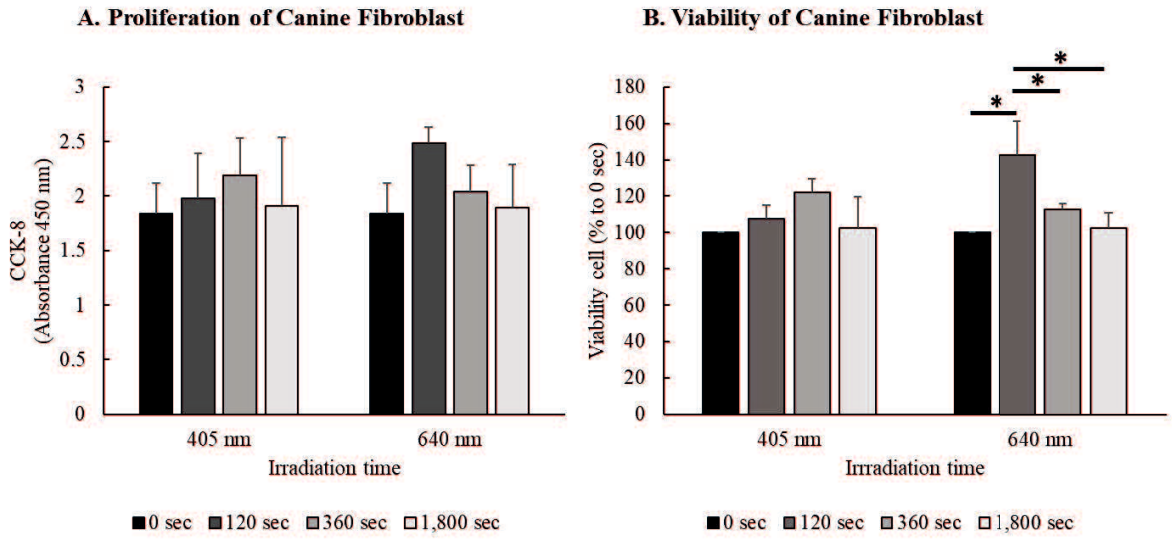

Figure 3. 1 The proliferation (A) and viability (B) of canine oral mucosa fibroblasts (using CCK-8 assay) were measured 24 hours after irradiation with single-dose LLL irradiation at wavelengths of 405 and 640 nm for 120, 360, and 1,800-sec. Proliferating fibroblasts are expressed as absorbance with optical density value, whereas the cell viability of fibroblasts is expressed as a percentage. The mean was compared by analysis of variance followed by Tukey's honestly significant difference test. All experiments were performed thrice for repeatability. *P < 0.05. CCK-8, Cell Counting Kit-8; LLL, low-level laser

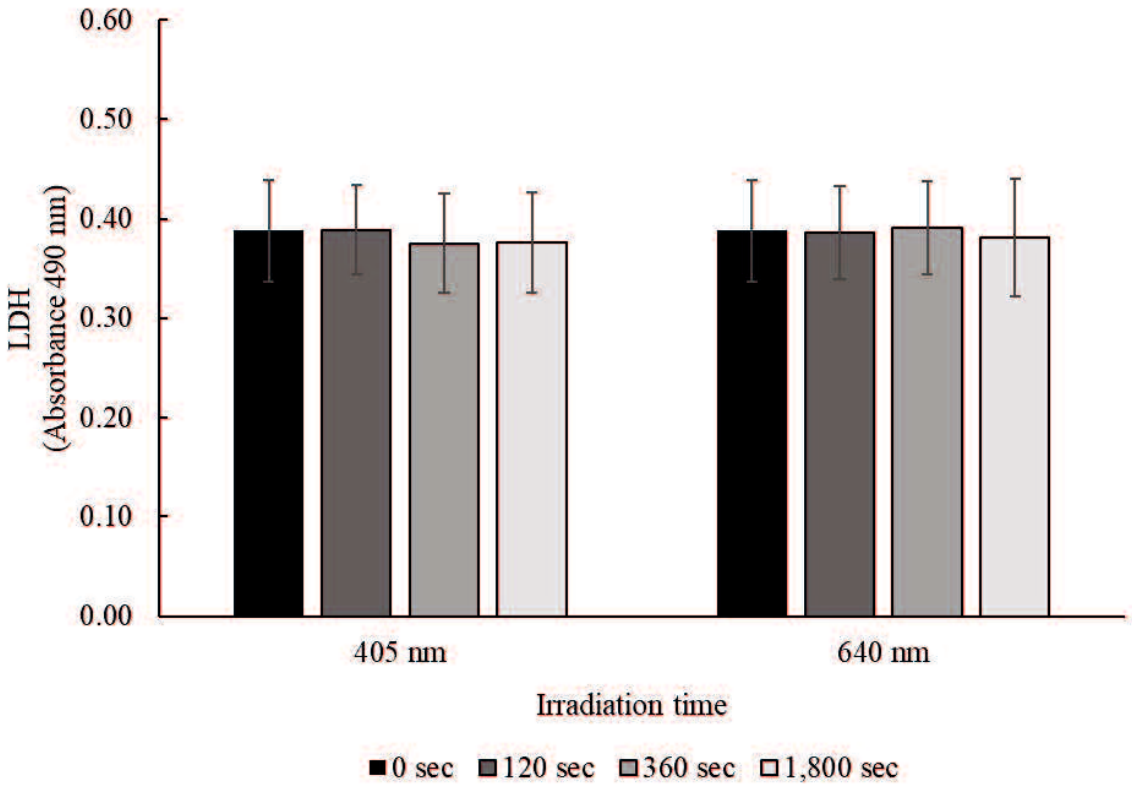

Figure 3. 2 The absorbance of LDH assay in canine oral mucosa fibroblasts at 24 hours after being treated with single-dose LLL irradiation at 405 and 640 nm wavelengths for 120, 360, and 1,800 sec. LDH is expressed as absorbance with optical density value. The mean was compared by analysis of variance followed by Tukey's honestly significant difference test. All experiments were performed thrice for repeatability. LDH, lactate dehydrogenase; LLL, low-level laser.

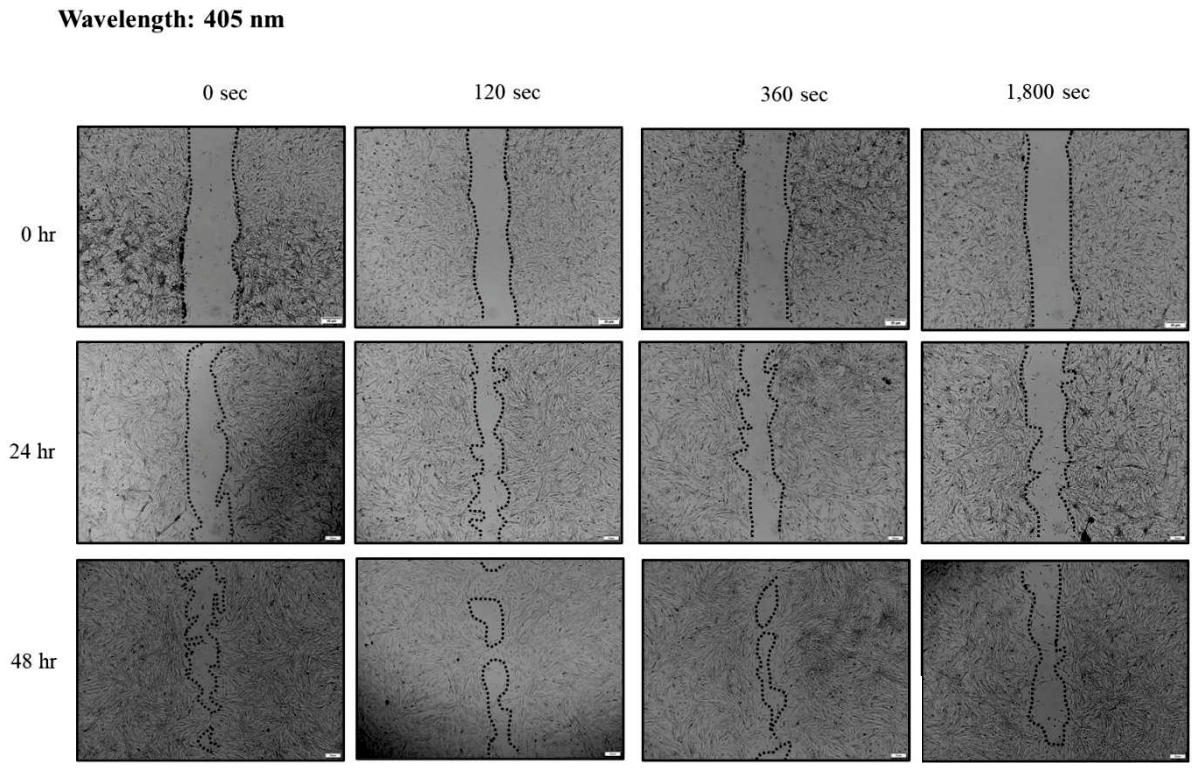

Figure 3. 3 Scratch assay evaluation at a wavelength of 405. Dotted lines indicate the scratch area at 0, 24, and 48 hours after laser irradiation. Fibroblasts that were irradiated for 360-sec showed the narrowest scratch at 48 hours. Scale bars = 20 μm.

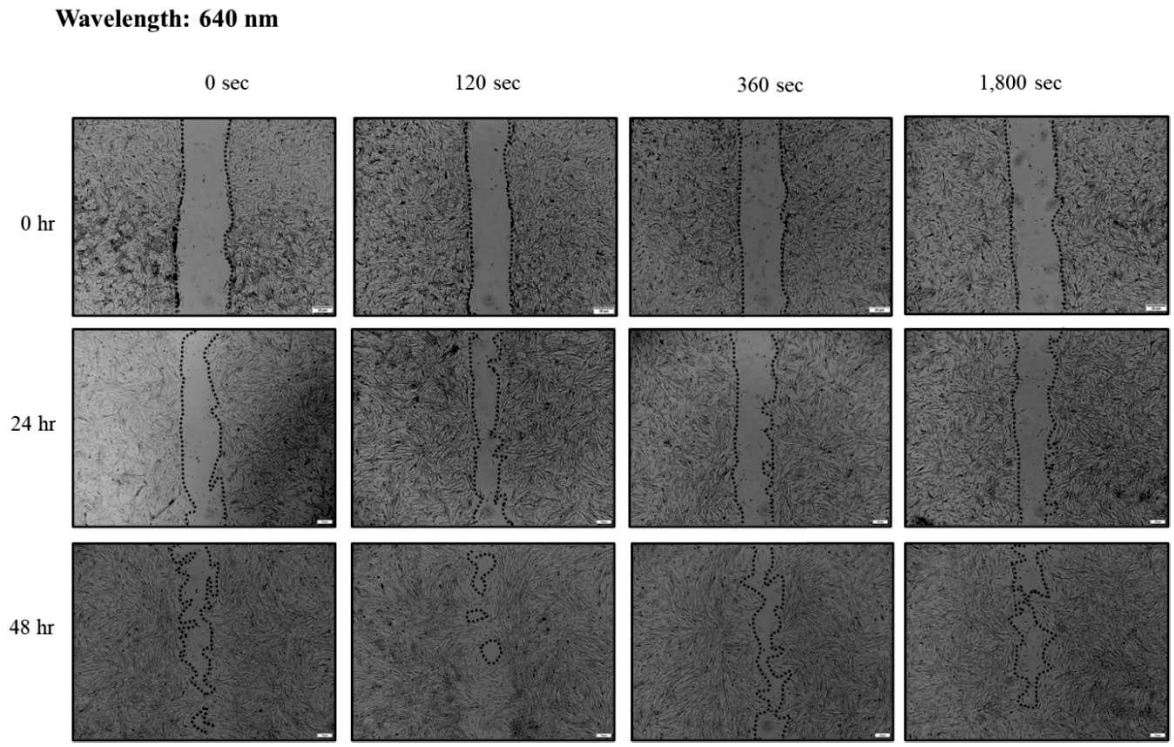

Figure 3. 4 Scratch assay evaluation at a wavelength of 640. Dotted lines indicate the scratch area at 0, 24, and 48 hours after laser irradiation. Fibroblasts that were irradiated for 120-sec showed the narrowest scratch at 48 hours. Scale bars = 20 μm.

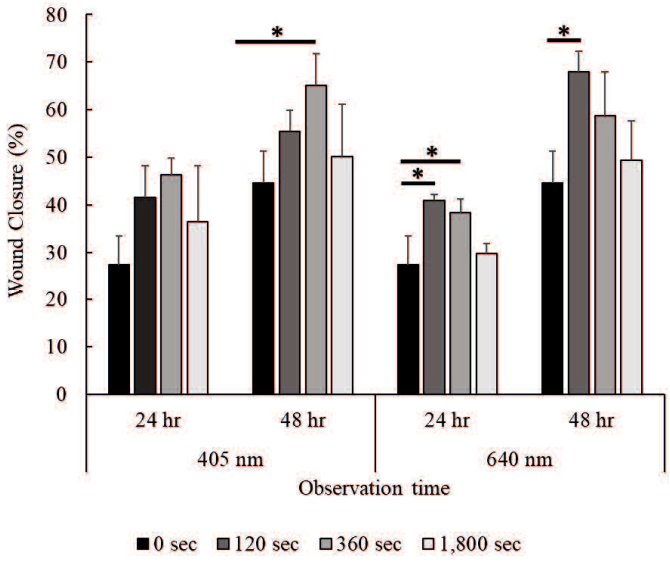

Figure 3. 5 Effects of LLL therapy at 405 and 640 nm wavelengths on cell migration. The scratch wound area was measured at 0, 24, and 48 hours after laser irradiation. *P < 0.05 represents statistically significant differences between irradiated and non-irradiated groups (control). LLL, low-level laser

CHAPTER IV

Effects of low-level laser therapy on canine multilayered fibroblast sheet

4.1 Abstract

Cell sheets represent an innovative tissue engineering approach, particularly in regenerative medicine. They create a sheet-like structure of cells that retains essential extracellular matrix components and cell-cell interactions, enhancing tissue repair and regeneration. Low-level laser (LLL) therapy is a non-invasive treatment modality that utilizes low-intensity lasers to stimulate cellular processes in wound healing. Introducing a combination of fibroblast sheets and LLL therapy may significantly improve the quality of treatment. This study aimed to investigate the effect of low-level laser irradiation on canine oral mucosal fibroblast sheets. The cell sheet was produced using a canine oral mucosal fibroblast. The LLL irradiation was performed using the Erchonia® EVL dual-diode laser at wavelengths of 405 nm (5 mW) at energy densities 0.17 and 0.51 J/cm^2 and 640 nm (7.5 mW) at energy densities 0.26 and 0.77 J/cm^2 in six groups of experiment parameters. Lactate dehydrogenase and the thickness of the sheets were evaluated. LLL therapy influences the thickness of the fibroblast sheet, suggesting its potential to enhance the proliferation of cells. The thickness of the sheet was increased in group 4 with one-time irradiation in five days of culturing in all irradiation doses. Importantly, all the irradiation groups at each energy density did not induce a higher cytotoxicity level than non-irradiation groups, demonstrating the safety of the LLL therapy. These findings suggest that LLL irradiation enhanced the thickness of the fibroblast sheet and was safely employed to produce the sheets.

4.2 Introduction

Cell sheet engineering is an advanced tissue engineering technique in regenerative medicine focused on repairing or replacing damaged tissue and organs using various biological techniques (Thummarati *et al*., 2023). Cell sheets are formed through self-assembly, allowing for high cell density and retention of extracellular matrix (ECM) components, which are crucial

for tissue integration (Hu *et al*., 2023). This technique is significant for regenerative medicine and has potential clinical applications across various medical conditions (Chang *et al.*, 2023). Cell sheets in animals showed effectiveness, including reinforcing the bronchial stump (Yoshimine *et al*., 2022), esophageal reconstruction (Yamamoto *et al*., 2023), regenerating mouse submandibular glands (Nam *et al*., 2019), preventing postoperative pancreatic fistula in rats (Iwamoto *et al*., 2021), and prevent perforation after duodenal endoscopic submucosal dissection in a porcine model (Matsumoto *et al*., 2020).

Low-level laser (LLL) therapy in the visible to the near-infrared spectral band (390–1,100 nm) is the absorption of laser light at the electronic level without the generation of heat (AlGhamdi *et al*., 2011; Mussttaf *et al*., 2019; Peplow *et al*., 2010). It may be applied in various treatments, including wound healing, inflammation, and pain reduction (Musssaff *et al*., 2019; Avci *et al*., 2013). LLL therapy stimulates cellular processes, enhancing ATP production and reducing oxidative stress (Wickenheisser *et al*., 2019; Pedroni *et al*., 2018). A significant finding is the variability in LLL therapy application methods, including differences in laser type, dosage, and wavelength (Wickenheisser *et al*., 2019). The wavelength of visible light varies from 400 nm to 700 nm, and was divided into blue /violet (400–500 nm), green (500–565 nm), yellow (565–590 nm), orange (590–625 nm), and red (625–700 nm) (Prado *et al*., 2023). The power output of lasers is 0.001 to 0.1 Watts with a range of length 300 up to 10,600 nm with energy density from 0.01 to 100 J/cm^2 (Posten *et al*., 2005; AlGhamdi *et al*., 2011; Avci *et al*., 2013; Prado *et al*., 2023). Previous studies reported that LLL therapy showed a significant role, including enhancing the bone healing process (Berni *et al*., 2023; Barale *et al*., 2020), chronic wounds (Hoisang *et al*., 2021), and neurodegenerative diseases (Abijo *et al*., 2023; Shen *et al*., 2024). In addition, LLL therapy has been shown to influence the activity of several growth factors, which are crucial for various cellular functions such as proliferation and healing (Rola *et al.,* 2022).

Our previous study found that the autologous transplantation of fibroblast sheets in dogs after lobectomy formed the connective tissue higher than in the control group (without sheet transplantation), indicating that the fibroblast sheet stimulates wound healing and prevents leakage postoperative. Fibroblasts are essential for secreting ECM components, which are crucial during tissue development, homeostasis, tissue repair, and collagen formation (Lendahl *et al*., 2022; Cialdai *et al*., 2022; Plikus *et al*., 2021; Jere and Houreld, 2024). LLL therapy enhances fibroblast cell proliferation and migration, stimulates protein synthesis, and releases growth factors essential for effective wound healing (Jere and Houreld, 2024; Bakshi *et al*., 2022; Gong *et al*., 2022; Solmaz *et al*., 2017). The previous studies reported that the fibroblast sheet has a significant potential in wound healing (Ike *et al*., 2022; Matsuno *et al*., 2022; Kanzaki *et al*., 2007; Yamamoto *et al*., 2023; Matsushima *et al*., 2016). Previously, we reported that LLL therapy using a dual-diode laser at wavelength 405 nm and 640 nm at an energy density of 0.26 to 0.51 J/cm^2 can stimulate the proliferation of canine fibroblasts. Thus, by introducing a combination of fibroblast sheet and LLL therapy, the quality of treatment may be improved.

To the best of our knowledge, there is no information about the effects of LLL irradiation in a canine fibroblast sheet. Thus, this study investigates the impact of low-level laser irradiation on canine oral mucosal fibroblast sheets. We hypothesized that LLL therapy using 405 and 640 nm wavelengths can improve the thickness of the canine fibroblast sheet without causing cell damage.

4.3 Material and Methods

4.3.1 Oral mucosa fibroblast cell culture

The Committee approved the protocol for collecting oral mucosal tissues on the Ethics

of Animal Experiments of Yamaguchi University, Japan (Protocol Number 484). Three healthy beagle dogs were utilized in this prospective study. The median age of the dogs was 6.5 (range: 6.2–6.7), with a mean body weight of 12.67 ± 1.15 kg. Collecting tissue was done under general anesthesia. The oral mucosal tissues were collected using a 6-mm biopsy trepan with a tissue thickness of 3 mm (BIOPSY PUNCH, Kai Industries Co., Ltd., Gifu, Japan) and were transported in a phosphate-buffered saline (PBS) containing antibiotics 100 U/mL penicillin and 100 μg/mL streptomycin (Penicillin-Streptomycin, Fujifilm Wako Pure Chemical Industries, Ltd., Osaka, Japan). The cells were isolated using 5,000 units of collagenase type I (Collagenase, Fujifilm Wako Pure Chemical Co., Ltd., Osaka, Japan) and cultured in Dulbecco's Modified Eagle Medium (DMEM®, Life Technologies Corporation, New York, NY, USA) with 10% fetal bovine serum (FBS) (FBS, Thermo Fisher Scientific Group, Tokyo, Japan), and 100 U/mL penicillin and 100 μg/mL streptomycin and were incubated overnight at 37°C under 5% CO_2. Isolation cells were collected and cultured with DMEM medium in an incubator for 3–5 days until fibroblast proliferation and adhesion were confirmed. Primary fibroblasts were seeded in a new DMEM in an uncoated T-75 flask (FALCON®, Corning International Inc., Tokyo, Japan) and cultured until the cells were 70%–80% confluent. The second passage of fibroblasts was used in the present study.

4.3.2 Preparation of fibroblast cell sheets

For the cell sheet preparation method, this study referred to the previous research. The cells were detached from the cell dish using TrypLE Express (TrypLE Express®, Life Technology Corporation, Grand Island, NY, USA), 10 μL of the cell suspension after centrifugation, and 10 μL of trypan blue were mixed and pipetted well. The cell numbers were counted using a Burker Turk cytometer. Primary fibroblast cells were seeded in a 24-well plate (5×10^5 cells/well) using a 2 mL medium consisting of DMEM and HFDM-1 (+) (Cell Science & Technology Institute, Miyagi, Japan) supplemented with 5% FBS. Ten μM Rho Kinase

(ROCK) inhibitors (Culture Sure®, Y-27632, Fujifilm Wako Pure Chemical Industries, Ltd., Osaka, Japan) were added to the wells. The surrounding wells without suspension cells were filled with 2 mL PBS to uniform the temperature and cultured for 3 and 5 days in an incubator at 37°C and 5% CO_2.

4.3.3 Laser irradiation

LLL irradiation was performed using the Erchonia® EVL dual-diode laser (Erchonia Corporation, Melbourne, FL, USA), which provides two laser diodes (405 nm [violet/blue laser beam] with an output of 5 mW and 640 nm [red laser beam] with an output of 7.5 mW). Each diode emits its wavelength with a tolerance of ±10 nm. Different groups were treated using two wavelengths (405 and 640 nm) with power output densities of 5 and 7.5 mW with energy densities of 0.17, 0.51, 0.26, and 0.77 J/cm^2 (Table 4.1). The energy density (J/cm^2) for all treatment groups was calculated by multiplying the exposure time (sec) by the laser's power output (W) divided by the surface area (cm^2). The surface area exposed to LLL therapy was identical to that of a 24-well plate (1.9 cm^2). The fibroblast suspension in the well plate without irradiation was treated similarly and used as a control. The laser's position was in contact with the bottom of the 12-well plate cover, with the laser beam placed at a 90° angle to the bottom of the 12-well plate, which was positioned in a stable supporting structure from Erchonia Corporation. LLL irradiation of group treatment and the collection time of fibroblast sheets were described in Table 4.2.

4.3.4 Lactate dehydrogenase (LDH) assay

The release of lactate dehydrogenase (LDH) was measured using a commercially available kit for measuring LDH (Cytotoxicity LDH Assay Kit-WST, Dojindo Laboratories, Kumamoto, Japan). The laser irradiation protocol was performed as previously described (Tables 4.1 and Table 4.2). The non-irradiated fibroblasts were used as a control group. The exposure medium was collected before sheet detachment. 100 µL of cell culture medium was

transferred into a 96-well plate and added with 100 μL of LDH reaction solution, prepared according to the manufacturer's guidelines. The plate was covered with foil and was incubated at room temperature for 30 minutes. Subsequently, 50 μL of stop solution was added, and the optical density of the solution was directly measured at 490 nm using an Epoch spectrophotometer (BioTek, Winooski, VT, USA). The LDH secretion data were presented as absorbance with optical density value.

4.3.5 Histological evaluation

The prepared cell sheet was detached by pipetting and fixed with formalin. The fibroblast sheets were placed on a raw ham to layer the sheet and embedded in paraffin. Sections with a thickness of 3 μm were cut and mounted on the glass slides, deparaffinized in xylene, and rehydrated in a graded ethanol series (100%, 90%, and 70%). The glass slide was stained with hematoxylin and eosin (H&E). For each fibroblast sheet slide, three figures were taken along the length of the sheet. Using ImageJ software (National Institutes of Health, MD, USA), four measurements were made per figure from the apical to the basal edge of the sheet.

4.3.6 Statistical analysis

Body weight was expressed as means ± standard deviation (SD) and age as median with range. LDH and thickness of the sheet were represented as the mean ± SD. The data were analyzed using a one-way analysis of variance followed by the Tukey–Kramer honestly significant difference test (for comparison of more than two groups). The calculations were performed using JMP software, version 9.0 (SAS Institute Japan, Tokyo, Japan). A P value < 0.05 is considered statistically significant for each test.

4.4 Results

4.4.1 Fibroblast sheets

Fibroblast sheets were detached 3 and 5 days after culturing. Fig 4.1 shows the

macroscopic appearance of fibroblast sheets immediately upon release of the cell culture well plate. Macroscopic observation of fibroblast sheets in all group treatments maintained a circular shape.

4.4.2 Lactate dehydrogenase (LDH) activity assay

The LDH activity of the fibroblast sheet was measured 3 days and 5 days after seeding the cells. In both time observations, there were no significant differences between the nonirradiated group (Groups 1 and 2) and the irradiated group (Groups 3, 4, 5, and 6) in each dose irradiation (0.17, 0.26, 0.51, and 0.77 J/cm^2) (Fig. 4.2 and Fig. 4.3). A slight increase in LDH release induced by LLL irradiation was found to be somewhat dose-dependent concerning the nonirradiated cells.

4.4.3 Sheet thickness evaluation

Hematoxylin and eosin staining were used to calculate the cell sheet thicknesses of the fibroblast sheet. The multilayered fibroblast sheet was successfully produced from oral mucosal fibroblasts with LLL irradiation at an energy density of 0.17 J/cm^2 (Fig.4.4), 0.26 J/cm^2 (Fig. 4.5), 0.51 J/cm^2 (Fig.4.6), and 0.77 J/cm^2 (Fig.4.7). Fibroblast sheet thickness at the energy density of 0.17 J/cm^2 (Fig. 4.8A) in groups 1, 2, 3, 4, 5, and 6 was 27.22 ± 3.60, 27.32 ± 2.97, 28.32 ± 5.42, 33.91 ± 4.11, 31.89 ± 3.46, and 28.65 ± 3.78 μm respectively. A significant difference was observed in group 4 compared to groups 2 and 3. Fibroblast sheet thickness at the energy density of 0.26 J/cm^2 (Fig. 4.8B) in groups 1, 2, 3, 4, 5, and 6 was 28.17 ± 5.23, 28.19 ± 2.99, 28.34 ± 5.11, 32.75 ± 3.21, 32.41 ± 5.4, and 26.1 ± 6.00 μm respectively. A significant difference was observed in groups 4 and 5 compared to group 6. Fibroblast sheet thickness at the energy density of 0.51 J/cm^2 (Fig. 4.8C) in groups 1, 2, 3, 4, 5, and 6 was 27.26 ± 1.24, 27.26 ± 2.43, 29.9 ± 1.96, 34.57 ± 5.32, 34.11 ± 5.99, and 29.49 ± 4.30 μm respectively. A significant difference was observed in groups 4 and 5 compared to nonirradiated groups (Groups 1 and 2). Fibroblast sheet thickness at the energy density of 0.77 J/cm^2 (Fig. 4.8D) in

groups 1, 2, 3, 4, 5, and 6 was 27.65 ± 6.87, 27.97 ± 3.1, 33.82 ± 7.15, 34.60 ± 3.33, 30/38 ± 4.54, and 28.53 ± 4.06 μm respectively. No significant difference was observed between the groups.

4.5 Discussion

This study represents the effects of LLL therapy on the thickness of the canine fibroblast sheet. LLL irradiation was applied during the formation of canine fibroblast cell sheets. Multilayered cell sheets with LLL irradiation increased the thickness of the sheet compared to nonirradiated sheets. The thickness of the sheet was increased in group 4 with one-time irradiation in five days of culturing in all irradiation doses. All the irradiation groups at each energy density did not induce a higher cytotoxicity level than non-irradiation groups. These findings suggest that LLL irradiation enhanced the thickness of the fibroblast sheet and was safely employed to produce the sheets.

Low-level laser therapy is a non-invasive technique that utilizes low-level light to enhance tissue regeneration, making it a valuable tool in tissue engineering. A previous study reported that LLL therapy improves cell survival rate in 3D tissue engineering applications (Bikmulina *et al*., 2022). LLL therapy has been effectively applied to various 3D systems, including hydrogel, steroids, cell sheets, and organoids, by enhancing cell viability (Bikmulina *et al*., 2022; Selestin Raja *et al*., 2024). LLL therapy stimulates mitochondrial activity and prevents cell death, enhancing cell viability and proliferation (Wickenheisser *et al*., 2019; Pedroni *et al*., 2018; Polina *et al*., 2022). LLL therapy has emerged as a significant technique in enhancing the efficacy of cell sheets for tissue regeneration. Selestin Raja *et al*. (2024) reported that LLL therapy's ability to promote tissue regeneration without needing external agents makes it a promising adjunct therapy in regenerative medicine. In the present study, the thickest layered sheets were found in all irradiated groups than in the non-irradiated groups,

which was expected. At energy density 0.17 J/cm^2, the irradiated sheet (group 4) significantly differed from the non-irradiated sheet (Group 1 and 2) for 3 and 5 days of culturing. At an energy density of 0.51 J/cm^2, the irradiated sheet (groups 4 and 5) significantly differed from both non-irradiated sheets. Meanwhile, at energy density 0.26 J/cm^2 and 0.77 J/cm^2, even though there was no significant difference, the results were in the same tendency as the 0.17 and 0.51 J/cm^2, which is the nonirradiated sheet was thinner compared to the irradiated groups. Our finding suggests that LLL therapy influences the thickness of the multilayered sheet. The sheet thickness is likely due to cell proliferation induced by LLL irradiation. Previous studies reported that LLL therapy stimulates cell proliferation (Hawkins and Abrahamse, 2007; Shingyochi *et al*., 2017; Gong *et al*., 2022; Solmaz *et al*., 2017). Our previous study reported that LLL therapy using a dual-diode laser at wavelength 405 nm and 640 nm at energy density 0.26 to 0.51 J/cm^2 can stimulate the proliferation of canine fibroblasts. The results were in line with the current study, which showed that LLL therapy increased the thickness of the fibroblast sheet at energy densities of 0.17, 0, 26, 0.51, and 0.77 J/cm^2.

Different LLL therapies, such as time and dose irradiation, can lead to varied outcomes in cell responses (Garrido *et al*., 2019; Ejiri *et al*., 2014; Ganjali *et al*., 2018). The biphasic dose response in LLL therapy indicates that low doses can stimulate biological processes, while higher doses may inhibit them (Alghamdi *et al*., 2011). This phenomenon is often described by the Arndt-Schulz law, which posits that weak stimuli enhance activity, moderate stimuli reach a peak effect, and excessive stimuli lead to suppression (Huang *et al*., 2009; Huang *et al*., 2011; Flores Luna *et al*., 2020). In the present study, we found that the sheet thickness in all irradiation groups in each dose irradiation was higher than in the non-irradiated group. We suggest that the LLL irradiation at energy density 0.17, 0.26. 0.51 and 0.77 J/cm^2 stimulate the proliferation of fibroblasts when forming the sheet.

In vitro studies reported that one-time irradiation (Nowak-Terpiłowska *et al*., 2023; Mathioudaki, 2024; Hou *et al*., 2008; Ginani *et al*., 2015) and repeated irradiation (Basso *et al*., 2012; Hawkins & Abrahamse, 2006; Almeida-Lopes *et al*., 2001; Ginani *et al*., 2017; Pevlov *et al.*, 2010) stimulate cell proliferation. Meanwhile, the in vivo studies reported that repeat LLL irradiation (Gong *et al*., 2022; Lou *et al*., 2019; Bayat *et al*., 2022) stimulates proliferation, tissue repair, and wound healing processes. To date, to our knowledge, no information compares the single and repeat doses in the canine fibroblast sheet. Thus, we evaluated the thickness of the sheet based on the time and frequency of irradiation. In each irradiation dose, our study showed the thickest sheet in group 4, where the irradiated cells were done the day after seeding, with culturing time for the fifth day (group 4). We suggest that single irradiation on the day after seeding with five days of culturing provide a thickness sheet that can potentially be used for clinical use.

Lactate dehydrogenase (LDH) is a crucial enzyme involved in cellular metabolism, particularly in converting pyruvate to lactate during anaerobic glycolysis. Its significance extends beyond essential metabolic functions, as elevated LDH levels are associated with various pathological conditions (Kabakov & Gabai, 2018). A previous study reported that LLL irradiation at different energy densities has positive, stimulating effects on the proliferation, secretion, and myogenic differentiation of BMSCs without cytotoxicity (Hou *et al*., 2008). Abrahamse and Crous (2024) reported that LLL irradiation did not induce apoptosis or indicate severe harm to the cells. Since LDH release serves as an indicator of disturbances of in-cell membrane integrity caused by pathological conditions, we evaluate this parameter in the culture medium to verify if the fibroblast sheet for 3 and 5 days followed by laser irradiation had deleterious effects on fibroblast membrane permeability. LDH levels in fibroblast sheet medium were similar in the groups in each dose irradiation for 3 and 5 days, and there were no significant differences between the groups in each dose irradiation. Both blue (405 nm) and red

(640 nm) LLL did not show cytotoxic effects. This result aligns with our previous study, which found that LLL therapy in 405 nm and 640 nm had energy densities of 0.17, 0.26, and 0.51. and 0.77 J/cm^2 did not show significant differences between nonirradiated and irradiated fibroblasts. These results suggest that LLL irradiation did not alter the cell membrane permeability of fibroblast and fibroblast sheets.

The exact mechanism of LLL therapy in forming the fibroblast sheet is still unclear and is likely multifactorial. While LLL therapy shows the potential to enhance the thickness of the multilayered fibroblast sheet, it is essential to consider the variability in responses based on treatment parameters. Previous studies reported that LLL therapy in cell sheets detected the presence of collagen type I and type III and fibronectin (Garrido *et al*., 2019; Pedroni *et al*., 2018). In 3D tissue engineering, Bikmulina *et al*. (2022) summarized the great potential of LLL therapy in stimulating cell survival and viability in 3D conditions. Therefore, further studies should investigate these parameters in canine fibroblast sheets.

4.6 Conclusion

This study set out to determine the impact of LLL irradiation on the canine fibroblast sheet. This research extends our knowledge about combination therapy and its implementation in producing the canine fibroblast sheet. The evidence from the present study suggests that fibroblast sheet fabrication with LLL irradiation could increase the thickness of the sheet without any substantial cytotoxicity

4.7 Tables Chapter IV

Table 4. 1 Characteristics of the low-level laser equipment

Wavelength (nm)	Energy Density (J/cm^2)	Power (mW)	Surface area (cm^2)	Total power (J)	Irradiation time (sec)
405	0.17	5	1.9	0.32	65
405	0.51	5	1.9	0.98	195
640	0.26	7.5	1.9	0.49	65
640	0.77	7.5	1.9	1.47	195

Table 4. 2 Group treatment of low-level laser therapy canine oral mucosal fibroblast sheet

Group	**Days**				
	1st	**2nd**	**3rd**	**4th**	**5th**
Group 1	Cell seeding	-	Detaching cell sheet	-	-
Group 2	Cell seeding	-	Medium changed	-	Detaching cell sheet
Group 3	Cell seeding	LLLI	Detaching cell sheet	-	-
Group 4	Cell seeding	LLLI	Medium changed	-	Detaching cell sheet
Group 5	Cell seeding	LLLI	Medium changed→LLLI	-	Detaching cell sheet
Group 6	Cell seeding	-	Medium changed→LLLI	-	Detaching cell sheet

LLLI: Low-level laser irradiation

4.8 Figures Chapter IV

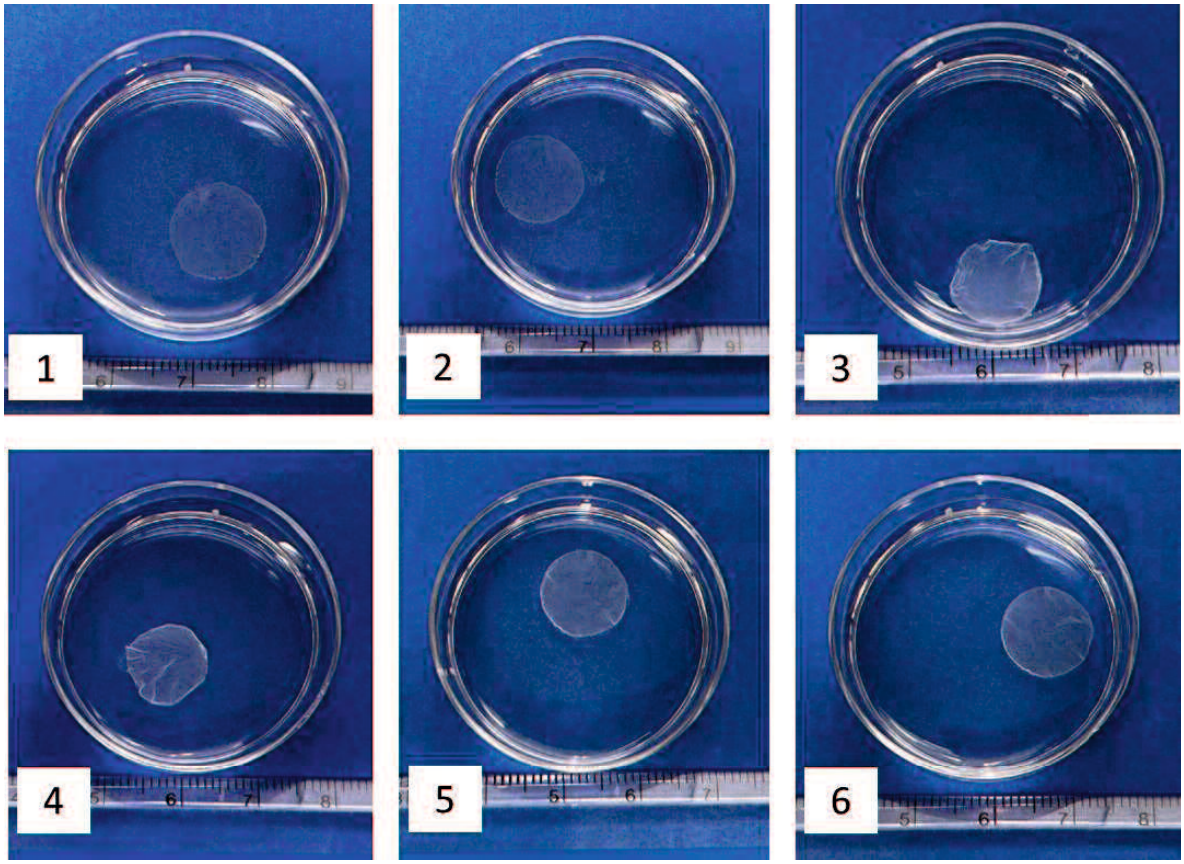

Figure 4. 1 Photograph of the fibroblast sheets immediately after detachment from the 24-well plate on a 60 mm culture dish. (1) control 3 days, (2) control 5 days, (3) group 4 at energy density 0.17 J/cm^2, (4) group 4 at energy density 0.26 J/cm^2, (5) group 4 at energy density 0.51 J/cm^2, (6) group 4 at energy density 0.77 J/cm^2

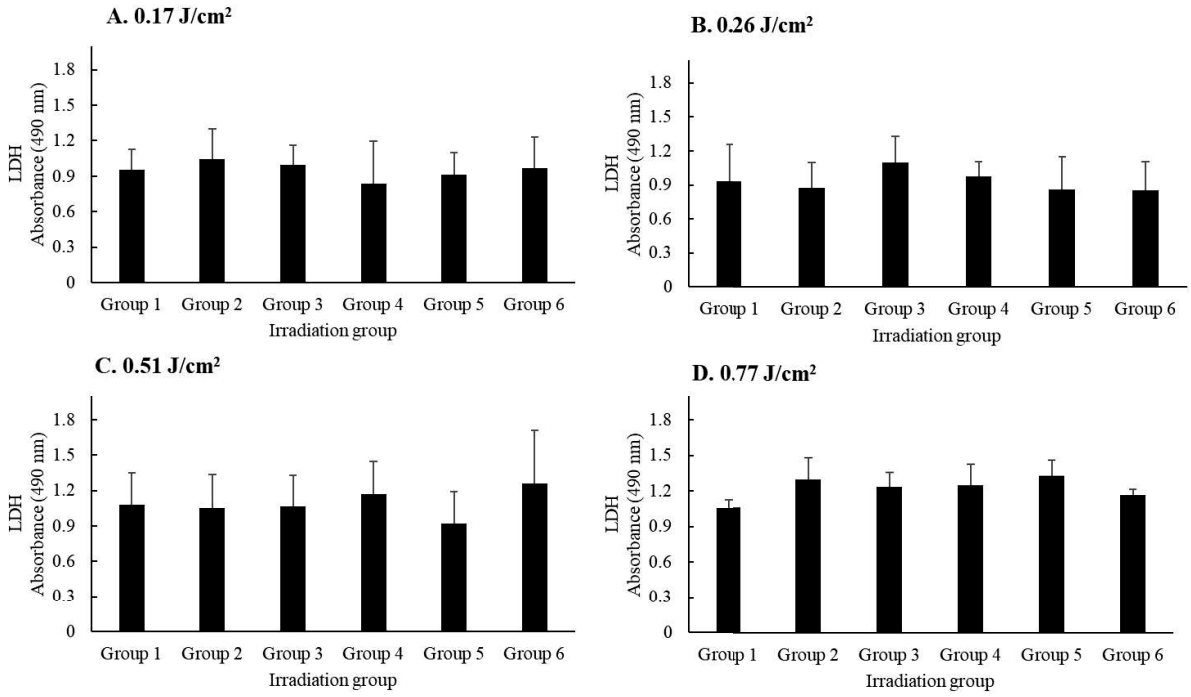

Figure 4. 2 LDH activity in canine fibroblast sheet at 3 days. No significant differences exist between the nonirradiated group (Groups 1 and 2) and the irradiated group (Groups 3, 4, 5, and 6) in each dose irradiation

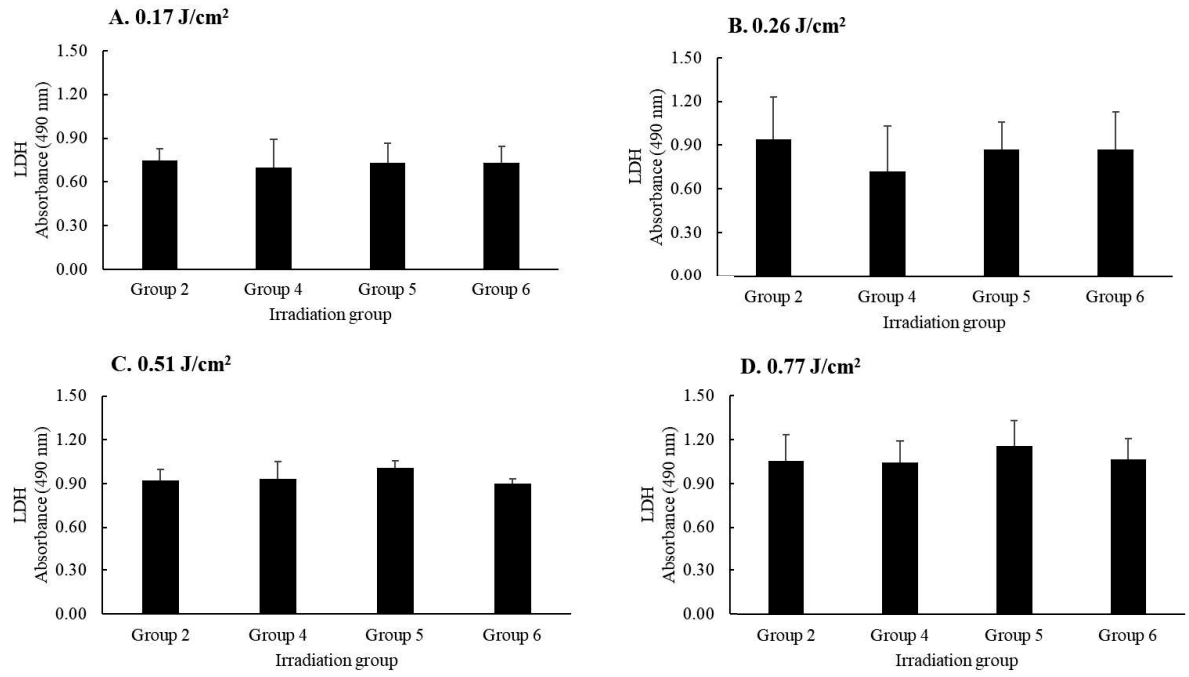

Figure 4. 3 LDH activity in canine fibroblast sheet at 5 days . No significant differences exist between the nonirradiated group (Groups 1 and 2) and the irradiated group (Groups 3, 4, 5, and 6) in each dose irradiation. Error bars represent means ± SD. *P < 0.05.

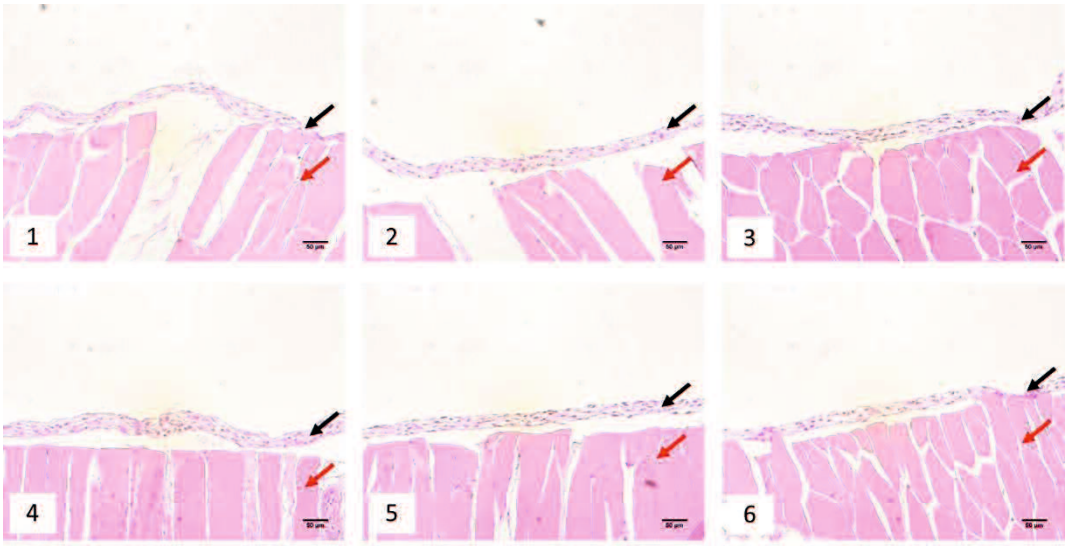

Figure 4. 4 Effects of LLL irradiation (0.17 J/cm^2) on construct thickness of fibroblast sheet. Representative cross-sectional H&E staining fibroblast sheet at an energy density of 0.17 J/cm^2 for (1) group 1, (2) group 2, (3) group 3, (4) group 4, (5) group 5, and (6) group 6. Black arrow: Marker for the fibroblast sheet. Red arrow: Marker for the raw ham. Scale bars = 50 μm.

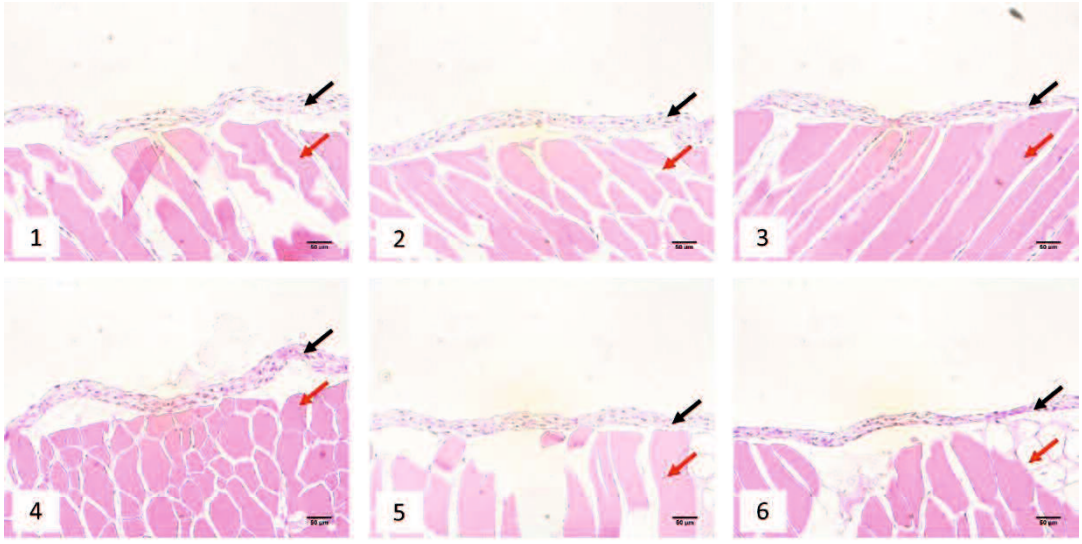

Figure 4. 5 Effects of LLL irradiation (0.26 J/cm^2) on construct thickness of fibroblast sheet. Representative cross-sectional H&E staining fibroblast sheet at an energy density of 0.26 J/cm^2 for (1) group 1, (2) group 2, (3) group 3, (4) group 4, (5) group 5, and (6) group 6. Black arrow: Marker for the fibroblast sheet. Red arrow: Marker for the raw ham. Scale bars = 50 μm.

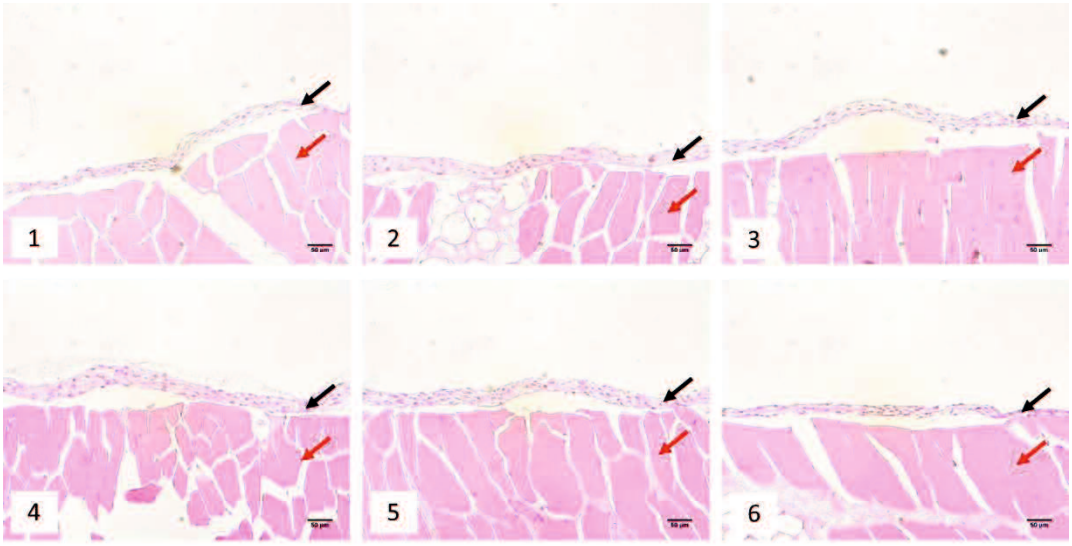

Figure 4. 6 Effects of LLL irradiation (0.51 J/cm^2) on construct thickness of fibroblast sheet. Representative cross-sectional H&E staining fibroblast sheet at an energy density of 0.51 J/cm^2 for (1) group 1, (2) group 2, (3) group 3, (4) group 4, (5) group 5, and (6) group 6. Black arrow: Marker for the fibroblast sheet. Red arrow: Marker for the raw ham. Scale bars = 50 μm.

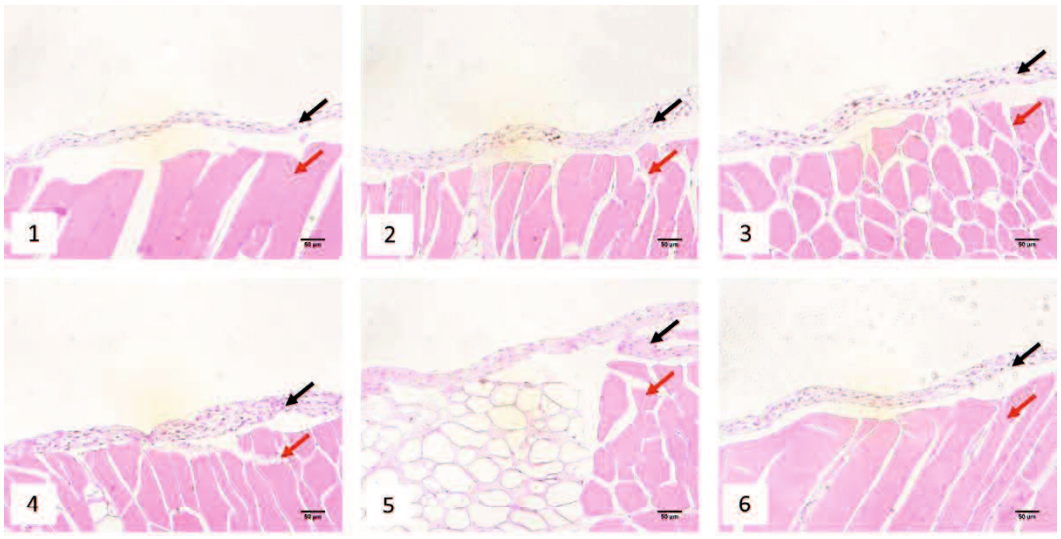

Figure 4. 7 Effects of LLL irradiation (0.77 J/cm^2) on construct thickness of fibroblast sheet. Representative cross-sectional H&E staining fibroblast sheet at an energy density of 0.77 J/cm^2 for (1) group 1, (2) group 2, (3) group 3, (4) group 4, (5) group 5, and (6) group 6. Black arrow: Marker for the fibroblast sheet. Red arrow: Marker for the raw ham. Scale bars = 50 μm.

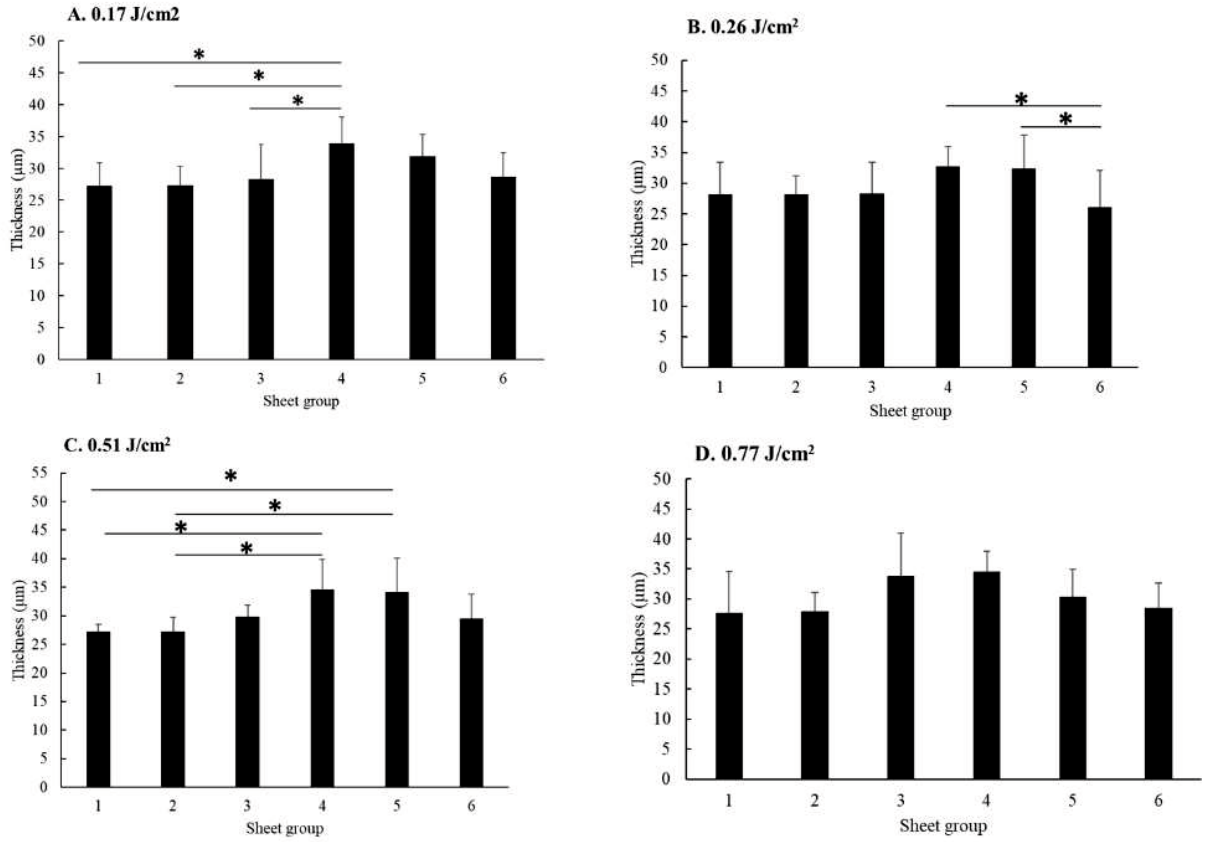

Figure 4. 8 The effect of LLL irradiation on the fibroblast sheet thickness. A: Fibroblast sheet thickness in nonirradiated groups (1 and 2) and irradiated groups (3, 4, 5, and 6) at the energy density of 0.17 J/cm^2. Group 4 had significant differences compared to groups 1, 2 and 3. B: Fibroblast sheet thickness in nonirradiated groups (1 and 2) and irradiated groups (3, 4, 5, and 6) at the energy density of 0.26 J/cm^2. Groups 4 and 5 had significant differences compared to Group 6. C: Fibroblast sheet thickness in nonirradiated groups (1 and 2) and irradiated groups (3, 4, 5, and 6) at the energy density of 0.51 J/cm^2. Groups 4 and 5 differed significantly from the unirradiated groups (1 and 2). Fibroblast sheet thickness in nonirradiated groups (1 and 2) and irradiated groups (3, 4, 5, and 6) at the energy density of 0.77 J/cm^2. Error bars represent means ± SD. *P < 0.05

GENERAL DISCUSSION

A method for producing a canine multilayered fibroblast sheet was successfully established using large numbers of fibroblast with ROCK inhibitors. According to fibroblast origin, canine oral mucosa fibroblasts are more potent than canine skin and tail skin fibroblasts. Oral mucosal fibroblast function continued to be investigated using low-level laser therapy. The Erchonia® EVL dual-diode laser with two wavelengths (405 and 640 nm) stimulates the proliferation and migration of canine fibroblasts with an irradiation time of 120–360 sec without causing cytotoxicity. We suggest that a combination of fibroblast sheets and LLL therapy may significantly improve the quality of treatment. The thickness of the sheet was increased with LLL irradiation with one-time irradiation in five days of culturing in all irradiation doses. Significantly, all the irradiation groups at each energy density did not induce a higher cytotoxicity level than non-irradiation groups, demonstrating the safety of the LLL therapy. These findings suggest that LLL irradiation and cell sheets from fibroblast cells can potentially enhance wound healing in dogs.

The first chapter focused on establishing the canine multilayered fibroblast sheet from three different tissue origins. In terms of morphology under light microscope observation, the three origins presented a spindle-shaped form without any differences. The sheet was created according to the previous study (Yoshimine *et al*., 2022). By then, the cell sheet did not retain its circular shape, and the margin of the sheet collapsed. We suggested that this condition may occur due to the activity of myosin phosphorylation during sheet formation. Myosin phosphorylation is regulated by Rho kinase (ROCK). Therefore, a ROCK inhibitor was required to prevent the myosin phosphorylation activity during sheet formation. ROCK inhibitor evaluation by adding 2.5, 5, 10, 30, and 50 μM to oral mucosal fibroblast culture. We found that adding rho kinase inhibitor in 2.5 and 5 μM did not form a sheet, but it worked in 10, 30, and 50 μM groups. Histological evaluation showed that adding the appropriate 10 μM

of ROCK inhibitor is the thickest layered sheet. We noticed that the cell sheet became thinner as the amount of the Rho kinase inhibitor increased. The multilayered canine fibroblast sheet was produced using the same method and adding 10 μM of ROCK inhibitor. However, the effect of ROCK inhibitor on myosin phosphorylation regulation, which can produce the canine fibroblast sheet, was not investigated. Further studies should be performed to address the role of ROCK inhibitors in the formation of canine fibroblast sheets.

Since the multilayered fibroblast sheet was performed from the three origins of cells, H&E staining was performed to evaluate the layered cell sheet. The oral mucosa sheet group was significantly thicker than the skin and tail skin fibroblast sheets. This indicates that the oral mucosal tissue has the strong potential to be a source of fibroblasts to develop tissue engineering. Although not explicitly expressed on fibroblast, by using immunohistochemical evaluation, specific proteins, such as vimentin, Vim, and fibroblast-specific protein 1, have served as valuable markers to identify fibroblasts (Lendahl *et al*., 2022). In this study, all groups were positive for vimentin. The presence of vimentin in all the fibroblast sheet groups indicated that applying a fibroblast sheet in the wound can promote fibroblast proliferation and stimulate wound healing. As VEGF and MCP-1 play a role in wound healing processes, our study found that all groups of sheets revealed both parameters, indicating that the fibroblast sheet can stimulate the wound healing process.

We investigated the cell sheet function in dogs by autologously transplanting it to the dogs after a lobectomy. Cell sheet transplantation studies on various organs have been developed to prevent bronchopleural fistula (BPF) in animal models, including fibroblast sheets. BPF is a postoperative complication that is difficult to treat because of the incomplete healing of a bronchial stump (Imai *et al*., 2011) with a mortality rate estimated to be 12.5-71.2% (Okuda *et al*., 2017; Tokunaga *et al*., 2020; Di Maio *et al*., 2015). Previous study has reported fibroblast sheets' role in improving the bronchial fistula's structural integrity post-

lobectomy (Yoshimine *et al*., 2022). Yamamoto *et al.* (2023) reported that fibroblast sheets contribute to increasing collagen deposition, which is crucial for tissue strength and integrity. Our study evaluates the effect of the autologous transplantation of multilayered fibroblast sheets on bronchial stump healing in dogs. This study confirmed the effect of transplanted autologous fibroblast sheets at least 7 days postoperatively. In the present study, the excised bronchial wall of the membranous side of the transplantation group was thicker than the non-transplantation group. We confirmed the presence of collagen deposits in the transplanted group. Since fibroblasts are known to promote collagen deposition, multilayered fibroblast sheets also have the potential to encourage the deposition of collagen in wound healing. The usefulness of the fibroblast sheet transplantation of refractory bronchial stump may provide an option as a therapeutic or preventive method for various diseases.

Since this study used large numbers of cells to produce the sheet, we paid attention to the proliferation ability of cells. According to the three of fibroblast origin, the oral mucosal fibroblast has a significant proliferation. Therefore, we continued the study by using the oral mucosal fibroblast. Since LLL therapy was well-known for enhancing the proliferation of cells, an investigation of the proliferation of cells using LLL irradiation was conducted. We evaluated the effects of irradiation using two laser wavelengths on the cell viability and migration of canine oral mucosa fibroblasts (405 and 640 nm) at different irradiation times (120, 360, and 1,800 sec). Our finding indicates that laser therapy under these conditions stimulates the proliferation and migration of oral mucosa fibroblasts; it is not harmful and might be safely employed to irradiate canine oral mucosa fibroblasts. This finding showed that the laser with a 405 and 640 nm wavelength and a specific fluence rate could promote fibroblast proliferation and migration, both essential in normal wound healing processes. Among the irradiated groups, the group irradiated for 1,800 sec with energy densities of 2.5 and 3.9 J/cm^2 showed the slowest proliferation and wound closure rate, suggesting that the time and dose of irradiation are

essential to the cell response. Huang *et al*. (2009; 2011) summarized the biphasic dose responses in LLL therapy on culture cells in vitro, animal models in vivo, and clinical studies. Based on the three-dimensional model of the Arndt–Schulz curve, they suggest that too much power density and/or time may lead to the inhibition effect of LLL therapy. The concept of biphasic dose–response is essential in LLL therapy because of the large number of illumination parameters for each treatment and laser characteristic (AlGhamdi *et al*., 2011; Avci *et al*., 2013; Huang *et al*., 2009; Huang *et al*., 2011). Therefore, further study of LLL therapy in canine fibroblast cells was recommended with an energy density of 0.2-0.5 J/cm^2.

Our investigation continued to evaluate the effect of LLL therapy on canine fibroblast sheets. Both parameters play a role in wound healing; therefore, we want to explore whether LLL therapy using 405 and 640 nm wavelengths can improve the characteristics of the canine fibroblast sheet. The percentage of cytotoxicity 1 day after LLL irradiation at the energy of 0.17, 0.26, 0.51, and 0.77 J/cm2 in each group showed no significant differences between the irradiated and the nonirradiated group. However, a slight increase in LDH release induced by LLL irradiation was found to be somewhat dose-dependent concerning the nonirradiated cells. This result is in line with the previous study that LLL irradiation did not show a significant difference in the bone marrow mesenchymal stem cells that were irradiated with LLL irradiation with energy density 0, 0.5, 1, 2, and 5 J/cm^2 (Hou *et al*., 2008). In the present study, the thickest layered sheets were found in all irradiated groups than in the non-irradiated groups, which was expected. Our finding suggests that LLL therapy influences the thickness of the multilayered sheet. The sheet thickness is likely due to cell proliferation induced by LLL irradiation. Previous studies reported that LLL therapy stimulates cell proliferation (Hawkins and Abrahamse, 2007; Shingyochi *et al*., 2017; Gong *et al*., 2022; Solmaz *et al*., 2017). The evidence from the present study suggests that fibroblast sheet fabrication with LLL irradiation could increase the thickness of the sheet without any substantial cytotoxicity.

This doctoral thesis reported that the canine multilayered fibroblast sheet was established, and LLL irradiation enhanced the thickness of the sheet. Future studies are needed to investigate the effect of fibroblast sheets with LLL irradiation *in vivo*. This research would interest all readers interested in developing tissue engineering, especially for developing future regenerative medicine in the veterinary field.

ACKNOWLEDGMENT

All praise goes to Almighty God for His gracious guidance, which enabled me to complete my studies through all the difficulties over the past four years. I am so grateful to have had my student life at the Laboratory of Veterinary Surgery, Animal Medical Centre, Joint Graduate School of Veterinary Medicine, Yamaguchi University from 2021 to 2025.

I am deeply grateful to have Prof. KENJI TANI, DVM, PhD, as the main supervisor during my PhD studies in the Laboratory of Veterinary Surgery, Department of Clinical Veterinary Science, Yamaguchi University for his wholehearted guidance, advice, and inspiration. He allowed me to be his student, doing research as I wanted, and following his activities during the past 4 years at Yamaguchi Animal Center taught me a lot about surgical cases and diagnostic imaging.

I would like to gratefully acknowledge another member of the supervisory committee, Prof MUNEKAZU NAKAICHI, DVM, PhD, and Prof MAKOTO FUJIKI, DVM, PhD, for their kindness during my study. It is my pleasure to express my sincere gratitude to HIROSHI SUNAHARA, DVM, PhD, YUKI NEMOTO, DVM, PhD, HARUMICHI ITOH, DVM, PhD, and KAZUHITO ITAMOTO, DVM, PhD for their patience and tireless tutoring during my study in the laboratory and animal hospital.

I want to express my deep gratitude to all current and former Laboratory of Veterinary Surgery students for their assistance, technical support, and scientific collaboration during my research. I also want to express my sincere gratitude to all members of the Animal Medical Centre of Yamaguchi University, a second home for my student life. I am thankful to the staff members of the United Graduate School of Veterinary Science's office and the International Support Center of Yamaguchi University for their cooperation in preparing the necessary documents.

I am honored to have been awarded the scholarship by the Ministry of Education, Culture, Sports, Science and Technology (Monbukagakusho) of Japan, which allowed me to pursue my studies and research at Yamaguchi University.

I want to thank Prof. DENI NOVIANA, DVM, PhD, and DaICVIM, who have always encouraged and supported me in continuously learning. I want to express my sincere gratitude to my BELOVED FAMILY for giving me the freedom to study abroad without any excuses; their never-ending support has been crucial in helping me achieve the highest level of success in my studies. Last, I would like to express my most profound thankfulness to myself for making it this far despite all the limitations and shortcomings. Thank you to all my friends who have supported me until this time. I hope the result of this study will be helpful in the veterinary field.

Melpa Susanti Purba

REFERENCES

1. Abijo A, Lee CY, Huang CY, Ho PC, Tsai KJ. 2023. The Beneficial Role of Photobiomodulation in Neurodegenerative Diseases. *Biomedicines* **11**: 1828.
2. Abrahamse H, Crous A. 2024. Photobiomodulation effects on neuronal transdifferentiation of immortalized adipose-derived mesenchymal stem cells. *Lasers Med Sci* **39**: 257.
3. Adtani P, Narasimhan M, Ranganathan K, Punnoose A, Prasad P, Natarajan PM. 2019. Characterization of oral fibroblasts: An in vitro model for oral fibrosis. *J Oral Maxillofac Pathol* **23**: 198–202.
4. Alfonso García, S. L., Parada-Sanchez, M. T., and Arboleda Toro, D. 2020. The phenotype of gingival fibroblasts and their potential use in advanced therapies. *Eur J Cell Biol* **99**: 151123.
5. AlGhamdi KM, Kumar A, Moussa NA. 2011. Low-level laser therapy: a valuable technique for enhancing the proliferation of various cultured cells. *Lasers Med Sci* **27**: 237–249.
6. Almeida-Lopes L, Rigau J, Zângaro RA, Guidugli-Neto J, Jaeger MM. 2001. Comparison of the low-level laser therapy effects on cultured human gingival fibroblast proliferation using different irradiance and same fluence. *Lasers in Surgery and Medicine* **29**: 179–184.
7. Álvarez-Santos, M. D., Álvarez-González, M., Estrada-Soto, S., and Bazán-Perkins, B. 2020. Regulation of myosin light-chain phosphatase activity to generate airway smooth muscle hypercontractility. *Front Physiol* **11**: 701
8. Apte RS, Chen DS, Ferrara N. 2019. VEGF in Signaling and Disease: Beyond Discovery and Development. *Cell* **176**: 1248–1264.
9. Arcerito, S., Manusia, M., Palazzo, G., Finocchiaro, G. B., Costanzo, L., and Deodata, G. 1982. Ricerche sperimentali sull'impiego della suturatrice meccanica nella chiusura del

moncone bronchiale [Experimental studies on the use of the mechanical suture device in bronchial stump closure. *Minerva chirurgica* **37**: 31–38.

10. Arefieva TI, Sokolov VO, Pylaeva EA, Kukhtina NB, Potekhina AV, Ruleva NY, Sidorova MV, Bespalova ZhD, Azmuko AA, Krasnikova TL. 2012. Peptide fragments 29-40 of an amino acid sequence of monocyte chemoattractant protein-1 (MCP-1) stimulate monocyte migration in vivo and facilitate wound healing. *Dokl Biol Sci* **446**: 327–330.
11. Avci P, Gupta A, Sadasivam M, Vecchio D, Pam Z, Pam N, Hamblin MR. 2013. Low-level laser (light) therapy (LLLT) in skin: stimulating, healing, restoring. *Semin Cutan Med Surg* **32**: 41–52.
12. Bainbridge P. 2013. Wound healing and the role of fibroblasts. *J Wound Care* **22**: 407–412.
13. Bakshi PV, Setty SB, Kulkarni, MR. 2022. Photobiomodulation of human gingival fibroblasts with diode laser - A systematic review. *Journal of Indian Society of Periodontology* **26**: 5–12.
14. Barale L, Monticelli P, Raviola M, Adami C. 2020. Preliminary clinical experience of low-level laser therapy for treating canine osteoarthritis-associated pain: A retrospective investigation on 17 dogs. *Open Vet J* **10**: 116–119.
15. Basso FG, Pansani TN, Turrioni AP, Bagnato VS, Hebling J, de Souza Costa CA. 2012. In vitro wound healing improvement by low-level laser therapy application in cultured gingival fibroblasts. *Int J Dent* **2012**: 719452.
16. Bayat M, Albright R, Hamblin MR, Chien S. 2022. Impact of Blue Light Therapy on Wound Healing in Preclinical and Clinical Subjects: A Systematic Review. *J Lasers Med Sci* **13**: e69.
17. Benchaprathanphorn K, Sakulaue P, Siriwatwechakul W, Muangman P, Chinaroonchai K, Viravaidya-Pasuwat K. 2020. Preparation and characterization of human keratinocyte-fibroblast cell sheets constructed using PNIAM-co-AM grafted surfaces for burn wound

healing. *J Mater Sci Mater Med* **31**: 126.

18. Berni M, Brancato AM, Torriani C, Bina V, Annunziata S, Cornella E, Trucchi M, Jannelli E, Mosconi M, Gastaldi G, Caliogna L, Grassi FA, Pasta, G. 2023. The Role of Low-Level Laser Therapy in Bone Healing: Systematic Review. *J Mol Sci* **24**: 7094.
19. Bikmulina P, Kosheleva N, Shpichka A, Yusupov V, Gogvadze V, Rochev Y, Timashev P. 2022. Photobiomodulation in 3D tissue engineering. *J Biomed Opt* **27**: 090901.
20. Bof, A. M., Rapoport, A., Paulo, D. N., Leiro, L. C., Gomes, M. R., & Pando-Serrano, R. R. 2007. Comparative study of the resistance of manual and mechanical sutures in the bronchial stump of dogs submitted to left pneumonectomy. *JBP **33***: 141–147.
21. Chamchoy K, Pakotiprapha D, Pumirat P, Leartsakulpanich U, Boonyuen U. 2019. Application of WST-8 based colorimetric NAD(P)H detection for quantitative dehydrogenase assays. *BMC Biochem* **20**: 4.
22. Chang D, Yang X, Fan S, Fan T, Zhang M, Ono M. 2023. Engineering of MSCs sheet for preventing myocardial ischemia and for left ventricle remodeling. *Stem Cell Res Ther* **14**: 102.
23. Chen G, Qi Y, Niu L, DI T, Zhong J, Fang T, Yan W. 2015. Application of the cell sheet technique in tissue engineering. *Biomed Rep* **3**: 749–757.
24. Cheng F, Shen Y, Mohanasundaram P, Lindström M, Ivaska J, Ny T, Eriksson JE. 2016. Vimentin coordinates fibroblast proliferation and keratinocyte differentiation in wound healing via TGF-β-Slug signaling. *Proc Natl Acad Sci* **113**: E4320–E4327.
25. Chung H, Dai T, Sharma SK, Huang YY, Carroll JD, Hamblin MR. 2011. The nuts and bolts of low-level laser (light) therapy. *Ann Biomed Eng* **40**: 516–533.
26. Cialdai F, Risaliti C, Monici M. 2022. Role of fibroblasts in wound healing and tissue remodeling on Earth and in space. *Front Bioeng Biotechnol* **10**: 958381.
27. Coelho-Rato LS, Parvanian S, Modi MK, Eriksson JE. Vimentin is at the core of wound

healing. *Trends Cell Biol* **34**: 239–254.

28. Crisan B, Soritau O, Baciut M, Campian R, Crisan L, Baciut G. 2013. Influence of three laser wavelengths on human fibroblasts cell culture. *Lasers Med Sci* **28**: 457–463.
29. Croze RH, Thi WJ, Clegg DO. 2016. ROCK inhibition promotes attachment, proliferation, and wound closure in human embryonic stem cell-derived retinal pigmented epithelium. *Trans Vis Sci Tech* **5**: 7.
30. Deshmane SL, Kremlev S, Amini S, Sawaya BE. 2009. Monocyte chemoattractant protein-1 (MCP-1): an overview. *J Interferon Cytokine Res* **29**: 313–326.
31. Dini V, Romanelli M, Oranges T, Davini G, Janowska A. 2021. Blue light emission in the management of hard-to-heal wounds. *Ital J Dermatol Venerol* **156**: 709–713.
32. Ejiri K, Aoki A, Yamaguchi Y, Ohshima M, Izumi Y. 2014. High-frequency, low-level diode laser irradiation promotes the proliferation and migration of primary cultured human gingival epithelial cells. *Lasers Med Sci* **29**: 1339–1347.
33. Endo, S., Ikeda, N., Kondo, T., Nakajima, J., Kondo, H., Shimada, Y., Sato, M., Toyooka, S., Okada, Y., Sato, Y., Yoshino, I., Okada, M., Okumura, M., Chida, M., Fukuchi, E., and Miyata, H. 2019. Risk assessments for broncho-pleural fistula and respiratory failure after lung cancer surgery by National Clinical Database Japan. *General thoracic and cardiovascular surgery* **67**: 297–305.
34. Etemadi A, Taghavi Namin S, Hodjat M, Kosarieh E, Hakimiha N. 2020. Assessment of the photobiomodulation effect of a blue diode laser on the proliferation and migration of cultured human gingival fibroblast cells: a preliminary in vitro study. *J Lasers Med Sci* **11**: 491–496.
35. Evans DH, Abrahamse H. 2008. Efficacy of three different laser wavelength for in vitro wound healing. *Photodermatol Photoimmunol Photomed* **24**: 199–210.
36. Fan J, Schiemer T, Vaska A, Jahed V, Klavins K. 2024. Cell via cell viability assay changes

cellular metabolic characteristics by intervening with glycolysis and pentose phosphate pathway. *Chem Res Toxicol* **37**: 208–211.

37. Farabi B, Roster K, Hirani R, Tepper K, Atak MF, Safai B. 2024. The Efficacy of Stem Cells in Wound Healing: A Systematic Review. *Int J Mol Sci* **25**: 3006.
38. Fernández-Guarino M, Hernández-Bule ML, Bacci S. 2023. Cellular and molecular processes in wound healing. *Biomedicines* **11**: 2526.
39. Ferrara N. 2004. Vascular endothelial growth factor: basic science and clinical progress. *Endocr Rev* **25**: 581–611.
40. Flores Luna GL, de Andrade ALM, Brassolatti P, Bossini PS, Anibal FF, Parizotto NA, Leal ÂMO. 2020. Biphasic dose/response of photobiomodulation therapy on culture of human fibroblasts. *Photobiomodul Photomed Laser Surg* **38**: 413–418.
41. Flores MG, Hasegawa M, Yamato M, Takagi R, Okano T, Ishikawa I. 2008. Cementum-periodontal ligament complex regeneration using the cell sheet technique. *J Periodontal Res* **43**: 364–371.
42. Fujino A, Fuchimoto Y, Mori T, Kano M, Yamada Y, Ohno M, Baba Y, Isogawa N, Arai K, Yoshioka T, Abe M, Kanai N, Takagi R, Maeda M, Umezawa A. 2023. Evaluation of safety and efficacy of autologous oral mucosa-derived epithelial cell sheet transplantation for prevention of anastomotic restenosis in congenital esophageal atresia and congenital esophageal stenosis. *Stem Cell Res Ther* **14**: 86.
43. Ganjali M, Seifalian AM, Mozafari M. 2018. Effect of Laser Irradiation on Cell Cycle and Mitosis. *J Lasers Med Sci* **9**: 249–253.
44. Gao L, Nath SC, Jiao X, Zhou R, Nishikawa S, Krawetz R, Li X, Rancourt DE. 2019. Post-Passage rock inhibition induces cytoskeletal aberrations and apoptosis in Human embryonic stem cells. *Stem Cell Res* **41**: 101641.
45. Gao X, Xing D. 2009. Molecular mechanisms of cell proliferation induced by low power

laser irradiation. *J Biomed Sci* **16**: 4.

46. Garrido PR, Pedroni ACF, Cury DP, Moreira MS, Rosin F, Sarra G, Marques MM. 2019. Effects of photobiomodulation therapy on the extracellular matrix of human dental pulp cell sheets. *J Photochem Photobiol* B **194**: 149–157.
47. Ginani F, Soares DM, Barreto MP, Barboza CA. 2015. Effect of low-level laser therapy on mesenchymal stem cell proliferation: a systematic review. *Lasers Med Sci* **30**: 2189–2194.
48. Ginani F, Soares DM, Rocha HAO, Barboza CAG. 2017. Low-level laser irradiation promotes proliferation of cryopreserved adipose-derived stem cells. *Einstein (Sao Paulo)* **15**: 334–338.
49. Gomes RN, Manuel F, Nascimento DS. 2021. The bright side of fibroblasts: molecular signature and regenerative cues in major organs. *NPJ Regen Med* **6**: 43.
50. Gomez-de-Antonio, D., Zurita, M., Santos, M., Salas, I., Vaquero, J., & Varela, A. (2010). Stem cells and bronchial stump healing. *J Thorac Cardiovasc Surg* **140**: 1397–1401.
51. Gong C, Lu Y, Jia C, Xu N. 2022. Low-level green laser promotes wound healing after carbon dioxide fractional laser therapy. *J Cosmet Dermatol* **21**: 5696–5703.
52. Grada A, Otero-Vinas M, Prieto-Castrillo F, Obagi Z, Falanga V. 2017. Research techniques made simple: analysis of collective cell migration using the wound healing assay. *J Invest Dermatol* **137**: e11–e16.
53. Greco M, Guida G, Perlino E, Marra E, Quagliariello E. 1989. Increase in RNA and protein synthesis by mitochondria irradiated with helium-neon laser. *Biochem Biophys Res Commun* **163**: 1428–1434.
54. Hamblin MR. 2018. Mechanisms and mitochondrial redox signaling in photobiomodulation. *Photochem Photobiol* **94**: 199–212.
55. Hawkins D, Abrahamse H. 2006. Effect of multiple exposures of low-level laser therapy on the cellular responses of wounded human skin fibroblasts. *Photomedicine and laser*

surgery **24**: 705–714.

56. Hawkins DH, Abrahamse H. 2007. Time-dependent responses of wounded human skin fibroblasts following phototherapy. *J Photochem Photobiol B* **88**: 147–55.
57. Hoisang S, Kampa N, Seesupa S, Jitpean S. 2021. Assessment of wound area reduction on chronic wounds in dogs with photobiomodulation therapy: A randomized controlled clinical trial. *Vet World* **14**: 2251–2259.
58. Hou JF, Zhang H, Yuan X, Li J, Wei YJ, Hu SS. 2008. In vitro effects of low-level laser irradiation for bone marrow mesenchymal stem cells: proliferation, growth factors secretion and myogenic differentiation. *Lasers Surg Med* **40**: 726–733.
59. Hu D, Li X, Li J, Tong P, Li Z, Lin G, Sun Y, Wang J. 2023. The preclinical and clinical progress of cell sheet engineering in regenerative medicine. *Stem Cell Res Ther* **14**: 112.
60. Huang YY, Chen AC, Carroll JD, Hamblin MR. 2009. Biphasic dose response in low level light therapy. *Dose Response* **7**: 358–383.
61. Huang YY, Sharma SK, Carroll J, Hamblin MR. 2011. Biphasic dose response in low level light therapy - an update. *Dose Response* **9**: 602–618.
62. Ike S, Ueno K, Yanagihara M, Mizoguchi T, Harada T, Suehiro K, Kurazumi H, Suzuki R, Kondo T, Murata T, Shirasawa B, Morikage N, Hamano K.2022. Cryopreserved allogenic fibroblast sheets: development of a promising treatment for refractory skin ulcers. *Am J Transl Res* **14**: 3879–3892.
63. Imai, K., Matsuzaki, I., Minamiya, Y., Saito, H., Yoshida, S., Hirayama, K., Sawano, T., and Ogawa, J. 2011. Postoperative bronchial stump fistula after lobectomy: response to occlusion with polyglycolic acid mesh and fibrin glue via bronchoscopy. *General Thoracic and Cardiovascular Surgery* **59**: 771-774
64. Imamura H, Adachi T, Kin T, Ono S, Sakai Y, Adachi T, Soyama A, Hidaka M, Takatsuki M, Shapiro AMJ, Eguchi S. 2018. An engineered cell sheet composed of human islets and

human fibroblast, bone marrow-derived mesenchymal stem cells, or adipose-derived mesenchymal stem cells: An in vitro comparison study. *Islets* **10**: e1445948.

65. Itabashi Y, Miyoshi S, Kawaguchi H, Yuasa S, Tanimoto K, Furuta A, Shimizu T, Okano T, Fukuda K, Ogawa S. 2005. A new method for manufacturing cardiac cell sheets using fibrin-coated dishes and its electrophysiological studies by optical mapping. *Artif Organs* **29**: 95–103.
66. Iwamoto K, Saito T, Takemoto Y, Ueno K, Yanagihara M, Furuya-Kondo T, Kurazumi H, Tanaka Y, Taura Y, Harada E, Hamano K. 2021. Autologous transplantation of multilayered fibroblast sheets prevents postoperative pancreatic fistula by regulating fibrosis and angiogenesis. *Am J Transl Res* **13**:1257–1268.
67. Jere SW, Houreld NN. 2024. Photobiomodulation (PBM): a therapeutic technique targeting fibroblast cell regeneration and survival in diabetic wounds. *Front Photonics* **5**:1423280.
68. Johnson KE, Wilgus TA. 2014. Vascular Endothelial Growth Factor and Angiogenesis in the Regulation of Cutaneous Wound Repair. *Adv Wound Care (New Rochelle)* **3**: 647–661.
69. Kabakov AE, Gabai VL. 2018. Cell death and survival assays. *Methods Mol Biol* **1709**: 107-127.
70. Kalluri R. 2016. The biology and function of fibroblasts in cancer. *Nat Rev Cancer* **16**: 582–598.
71. Kaneko-Kawano T, Takasu F, Naoki H, Sakumura Y, Ishii S, Ueba T, Eiyama A, Okada A, Kawano Y, Suzuki K. 2012. Dynamic regulation of myosin light chain phosphorylation by Rho-kinase. *PLoS One* **7**: e39269.
72. Kanzaki M, Yamato M, Yang J, Sekine H, Kohno C, Takagi R, Hatakeyama H, Isaka T, Okano T, Onuki T. 2007. Dynamic sealing of lung air leaks by the transplantation of tissue engineered cell sheets. *Biomaterials*. **28**: 4294–4302.

73. Karu TI, Pyatibrat LV, Kolyakov SF, Afanasyeva NI. 2005. Absorption measurements of a cell monolayer relevant to phototherapy: reduction of cytochrome c oxidase under near IR radiation. *J Photochem Photobiol B* **81**: 98–106.

74. Kasai Y, Morino T, Mori E, Yamamoto K, Kojima H. 2020. ROCK inhibitor combined with Ca^{2+} controls the myosin II activation and optimizes human nasal epithelial cell sheets. *Sci Rep* **10**: 16853.

75. Kawasaki K, Shimizu N. 2000. Effects of low-energy laser irradiation on bone remodeling during experimental tooth movement in rats. *Lasers Surg Med* **26**: 282–291.

76. Kendall RT, Feghali-Bostwick CA. 2014. Fibroblasts in fibrosis: novel roles and mediators. *Front Pharmacol* **5**: 123.

77. Kim KW, Shin YJ, Lee SCS. 2022. Novel ROCK Inhibitors, Sovesudil and PHP-0961, Enhance Proliferation, Adhesion and Migration of Corneal Endothelial Cells. *Int J Mol Sci* **23**: 14690.

78. Kim SR, Yi HJ, Lee YN, Park JY, Hoffman RM, Okano T, Shim IK, Kim SC. 2018. Engineered mesenchymal stem-cell-sheets patches prevents postoperative pancreatic leakage in a rat model. *Sci Rep*. **8**: 360.

79. Kim SW, Im GB, Jeong GJ, Baik S, Hyun J, Kim YJ, Pang C, Jang YC, Bhang SH. 2021. Delivery of a spheroids-incorporated human dermal fibroblast sheet increases angiogenesis and M2 polarization for wound healing. *Biomaterials* **275**: 120954.

80. Kim SW, Seo I, Hyun J, Eom J, Um SH, Bhang SH. 2023. Fibronectin-Enriched Interface Using a Spheroid-Converged Cell Sheet for Effective Wound Healing. *ACS Appl Mater Interfaces* **15**: 11536–11548.

81. Kirby GTS, Michelmore A, Smith LE, Whittle JD, Short RD. 2018. Cell sheets in cell therapies. *Cytotherapy* **20**: 169–180.

82. Kreisler M, Christoffers AB, Willershausen B, d'Hoedt B. 2003. Effect of low-level

GaAlAs laser irradiation on the proliferation rate of human periodontal ligament fibroblasts: an in vitro study. *J Clin Periodontol* **30**: 353–358.

83. Lee HG, Eun HC. 1999. Differences between fibroblasts cultured from oral mucosa and normal skin: implication to wound healing. *J Dermatol Sci* **21**: 176–82.
84. Lee J, Shin D, Roh JL. 2018. Use of a pre-vascularised oral mucosal cell sheet for promoting cutaneous burn wound healing. *Theranostics* **8**: 5703–5712.
85. Lendahl U, Muhl L, Betsholtz C. 2022. Identification, discrimination and heterogeneity of fibroblasts. *Nat Commun* **13**:3409.
86. Li M, Ma J, Gao Y, Yang L. Cell sheet technology: a promising strategy in regenerative medicine. *Cytotherapy* **21**:3–16.
87. Liang CC, Park AY, Guan JL.2007. In vitro scratch assay: a convenient and inexpensive method for analysis of cell migration in vitro. *Nat Protoc* **2**: 329–333.
88. Llontop, P., Santana-Rodríguez, N., Clavo, B., Quintana, A., Fiuza, M. D., Camacho, R., Santana-Rodríguez, A., Santana, C., and Ruíz-Caballero, J. A. 2014. Stem cells protect the bronchial stump in rat, increasing Sox6, Col2a1, and Agc1 expression. *Lung* **192**: 441–448.
89. Lopez A, Brundage C. 2019. Wound photobiomodulation treatment outcomes in animal models. *J Vet Med* **2019**: 6320515.
90. Lou Z, Gong T, Kang J, Xue C, Ulmschneider C, Jiang JJ. 2019. The Effects of Photobiomodulation on Vocal Fold Wound Healing: In Vivo and In Vitro Studies. *Photobiomodul Photomed Laser Surg* **37**: 532–538.
91. Ma H, Yang J-P, Tan RK, Lee H-W, Han S-K. 2018. Effect of low-level laser therapy on proliferation and collagen synthesis of human fibroblasts in vitro. *J Wound Manag Res* **14**: 1–6.
92. MacLean J, Pasumarthi KBS. 2020. Characterization of primary adult mouse cardiac

fibroblast cultures. *Can J Physiol Pharmacol* **98**: 861–869.

93. Makidono, K., Miyata, Y., Ikeda, T., Tsutani, Y., Kushitani, K., Takeshima, Y., & Okada, M. 2020. Investigation of surgical technique for bronchial stump closure after lobectomy in animal model. *General thoracic and cardiovascular surgery* **68**: 609–614.
94. Mani S, Swargiary G. 2023. In vitro cytotoxicity analysis: mtt/xtt, trypan blue exclusion. In: animal cell culture: principles and practice. techniques in life science and biomedicine for the non-expert (Mani S, Singh M, Kumar A eds.), US: Springer, pp. 267–284.
95. Masson-Meyers DS, Bumah VV, Enwemeka CS. 2016. Blue light does not impair wound healing in vitro. *J Photochem Photobiol B* **160**: 53–60.
96. Mathioudaki E, Rallis M, Politopoulos K, Alexandratou E. 2024. Photobiomodulation and Wound Healing: Low-Level Laser Therapy at 661 nm in a Scratch Assay Keratinocyte Model. *Ann Biomed Eng* **52**: 376–385.
97. Matsumoto R, Kanetaka K, Maruya Y, Yamaguchi S, Kobayashi S, Miyamoto D, Ohnita K, Sakai Y, Hashiguchi K, Nakao K, Eguchi S. 2020. The Efficacy of Autologous Myoblast Sheet Transplantation to Prevent Perforation After Duodenal Endoscopic Submucosal Dissection in Porcine Model. *Cell Transplant* **29**: 963689720963882.
98. Matsumoto T, Kim MH, Kino-Oka M. 2022. Effect of Rho-Associated Kinase Inhibitor on Growth Behaviors of Human Induced Pluripotent Stem Cells in Suspension Culture. *Bioengineering (Basel)* **9**: 613.
99. Matsumura F, Totsukawa G, Yamakita Y, Yamashiro S. 2001. Role of myosin light chain phosphorylation in the regulation of cytokinesis. *Cell Struct Funct* **26**: 639–644.
100. Matsuno Y, Yanagihara M, Ueno K, Saito T, Kurazumi H, Suzuki R, Katsura S, Oga A, Hamano K. 2022. Dry preserved multilayered fibroblast cell sheets are a new manageable tool for regenerative medicine to promote wound healing. *Sci Rep* **12**: 12519.
101. Matsushima H, Kuroki T, Adachi T, Kitasato A, Ono S, Tanaka T, Hirabaru M, Kuroshima

N, Hirayama T, Sakai Y, Soyama A, Hidaka M, Takatsuki M, Kin T, Shapiro J, Eguchi S. 2016. Human Fibroblast Sheet Promotes Human Pancreatic Islet Survival and Function In Vitro. *Cell Transplant* **25**: 1525–1537.

102. McGifford OJ, Harkin DG, Cuttle L. 2022. Effect of Rho-Associated Protein Kinase Inhibitors on Epidermal Keratinocytes: A Proposed Application for Burn Wound Healing. *Tissue Eng Part B Rev* **28**: 555–568.

103. Mizoguchi T, Ueno K, Takeuchi Y, Samura M, Suzuki R, Murata T, Hosoyama T, Morikage N, Hamano K. 2018. Treatment of Cutaneous Ulcers with Multilayered Mixed Sheets of Autologous Fibroblasts and Peripheral Blood Mononuclear Cells. *Cell Physiol Biochem* **47**: 201–211.

104. Moore P, Ridgway TD, Higbee RG, Howard EW, Lucroy MD. 2005. Effect of wavelength on low-intensity laser irradiation-stimulated cell proliferation in vitro. *Lasers Surg Med* 36: 8–12.

105. Movat HZ, Fernando NV. 1962. The fine structure of connective tissue. I. The fibroblast. *Exp Mol Pathol* **1**: 509–534.

106. Murakami, J., Ueda, K., Hayashi, M., Sano, F., and Hamano, K. 2016. Simultaneous stapling of the lobar bronchus and pulmonary artery: is it actually dangerous?. *Interactive cardiovascular and thoracic surgery* **22**: 671–673.

107. Mussttaf RA, Jenkins DFL, Jha AN. 2019. Assessing the impact of low level laser therapy (LLLT) on biological systems: a review. *Int J Radiat Biol* **95**: 120–143.

108. Nagase T, Ueno K, Mizoguchi T, Samura M, Harada T, Suehiro K, Shirasawa B, Morikage N, Hamano K. 2020. Allogeneic fibroblast sheets accelerate cutaneous wound healing equivalent to autologous fibroblast sheets in mice. *Am J Transl Res* **12**: 2652–2663.

109. Nakayama M, Amano M, Katsumi A, Kaneko T, Kawabata S, Takefuji M, Kaibuchi K. 2005. Rho-kinase and myosin II activities are required for cell type and environment

specific migration. *Genes Cells* **10**: 107–117.

110. Nam K, Kim K, Dean SM, Brown CT, Davis RS, Okano T, Baker OJ. 2019. Using cell sheets to regenerate mouse submandibular glands. *NPJ Regen Med* **4**:16.

111. Niggli V. 1999. Rho-kinase in human neutrophils: a role in signalling for myosin light chain phosphorylation and cell migration. *FEBS letters* **445**: 69–72.

112. Nishimura A, Nakajima R, Takagi R, Zhou G, Suzuki D, Kiyama M, Nozaki T, Owaki T, Takahara T, Nagai S, Nakamura T, Sugaya M, Terada K, Igarashi Y, Hanzawa H, Okano T, Shimizu T, Yamato M, Takeda S. 2019. Fabrication of tissue-engineered cell sheets by automated cell culture equipment. *J Tissue Eng Regen Med* **13**: 2246–2255.

113. Nowak-Terpiłowska A, Zeyland J, Hryhorowicz M, Śledziński P, Wyganowska M. 2023. Influence of Three Laser Wavelengths with Different Power Densities on the Mitochondrial Activity of Human Gingival Fibroblasts in Cell Culture. *Life (Basel)* **13**:1136.

114. Okuda, M., Go, T., and Yokomise, H. 2017. Risk factor of bronchopleural fistula after general thoracic surgery: review article. *General thoracic and cardiovascular surgery* **65**: 679–685.

115. Okumura N, Kinoshita S, Koizumi N. 2017. Application of Rho Kinase Inhibitors for the Treatment of Corneal Endothelial Diseases. *J Ophthalmol* **2017**: 2646904.

116. Pakshir P, Noskovicova N, Lodyga M, Son DO, Schuster R, Goodwin A, Karvonen H, Hinz B. 2020. The myofibroblast at a glance. *J Cell Sci* **133**: jcs227900.

117. Panagopoulos, N. D., Apostolakis, E., Koletsis, E., Prokakis, C., Hountis, P., Sakellaropoulos, G., Bellenis, I., and Dougenis, D. 2009. Low incidence of bronchopleural fistula after pneumonectomy for lung cancer. *Interact Cardiovasc Thorac Surg* **9**: 571–575.

118. Pavlov S, Babenko N, Kumetchko M, Litvinova O, Komarchuk I. 2024. Activation of

reparative processes of chronic wounds using photobiomodulation therapy (experimental study). *Pol Merkur Lekarski* **52**: 261–267.

119. Pedroni ACF, Diniz IMA, Abe GL, Moreira MS, Sipert CR, Marques MM. 2018. Photobiomodulation therapy and vitamin C on longevity of cell sheets of human dental pulp stem cells. *J Cell Physiol* **233**: 7026-7035.

120. Peh GS, Adnan K, George BL, Ang HP, Seah XY, Tan DT, Mehta JS. 2015. The effects of Rho-associated kinase inhibitor Y-27632 on primary human corneal endothelial cells propagated using a dual media approach. *Sci Rep* **16**: 9167.

121. Peplow PV, Chung TY, Baxter GD. 2010. Laser photobiomodulation of proliferation of cells in culture: a review of human and animal studies. *Photomed Laser Surg* **1**: S3–S40.

122. Perego R, Mazzeo M, Spada E, Proverbio D. 2022. Critically appraised topic on low-level laser therapy (lllt) in dogs: an advisable treatment for skin diseases?. *Vet Sci* **9**: 505.

123. Perego R. 2016. First experience with photobiomodulation (pbm) in post-surgical wound healing in dogs. *JVCPC* **1**: 105.

124. Piltti J, Varjosalo M, Qu C, Häyrinen J, Lammi MJ. 2015. Rho-kinase inhibitor Y-27632 increases cellular proliferation and migration in human foreskin fibroblast cells. *Proteomics* **15**: 2953–2965.

125. Plikus MV, Wang X, Sinha S, Forte E, Thompson SM, Herzog EL, Driskell RR, Rosenthal N, Biernaskie J, Horsley V. 2021. Fibroblasts: Origins, definitions, and functions in health and disease. *Cell* **184**: 3852–3872.

126. Polina Y, Bikmulina, Nastasia V, Kosheleva, Anastasia, Shpichka, Vladimir, Yusupov, Vladimir, Gogvadze, Yury, Rochev P, Timashev. 2022. Photobiomodulation in 3D tissue engineering. *Journal of Biomedical Optics* **27**

127. Posten W, Wrone DA, Dover JS, Arndt KA, Silapunt S, Alam M. 2005. Low-level laser therapy for wound healing: mechanism and efficacy. *Dermatol Surg* **31**:334-340.

128. Prado TP, Zanchetta FC, Barbieri B, Aparecido C, Melo Lima MH, Araujo EP. 2023. Photobiomodulation with blue light on wound healing: a scoping review. *Life (Basel)* **13**: 575.

129. Ravikanth M, Soujanya P, Manjunath K, Saraswathi TR, Ramachandran CR. 2011. Heterogenecity of fibroblasts. *J Oral Maxillofac Pathol* **15**: 247–250.

130. Ridge KM, Eriksson JE, Pekny M, Goldman RD. 2022. Roles of vimentin in health and disease. *Genes Dev* **36**: 391–407.

131. Rinn JL, Bondre C, Gladstone HB, Brown PO, Chang HY. 2006. Anatomic demarcation by positional variation in fibroblast gene expression programs. *PLoS Genet*. **2**: e119.

132. Rodriguez LG, Wu X, Guan JL. 2005. Wound-healing assay. *Methods Mol Biol* **294**: 23–29.

133. Rola P, Włodarczak S, Lesiak M, Doroszko A, Włodarczak A. 2022. Changes in cell biology under the influence of low-level laser therapy. *Photonics* **9**: 502.

134. Roman J. 2023. Fibroblast-Warriors at the intersection of wound healing and disrepair. *Biomolecules* **13**: 945.

135. Rossi F, Magni G, Tatini F, Banchelli M, Cherchi F, Rossi M, Coppi E, Pugliese AM, Rossi degl'Innocenti D, Alfieri D, Pavone FS, Pini R, Matteini P. 2021. Photobiomodulation of human fibroblasts and keratinocytes with blue light: implications in wound healing. *Biomedicines* **9**: 41.

136. Sakai Y, Koike M, Hasegawa H, Yamanouchi K, Soyama A, Takatsuki M, Kuroki T, Ohashi K, Okano T, Eguchi S. 2023. Rapid fabricating technique for multi-layered human hepatic cell sheets by forceful contraction of the fibroblast monolayer. *PLoS One*. **8**: e70970.

137. Schartinger VH, Galvan O, Riechelmann H, Dudas J. 2012. Differential responses of fibroblasts, non-neoplastic epithelial cells, and oral carcinoma cells to low-level laser

therapy. *Support Care Cancer* **20**: 523–529.

138. Seasholtz TM. 2003. The RHOad less traveled: the myosin phosphorylation-independent path from Rho kinase to cell contraction. Focus on "Rho kinase mediates serum-induced contraction in fibroblast fibers independent of myosin LC20 phosphorylation". *Am J Physiol Cell Physiol* **284**: C596–C598.

139. Selestin Raja I, Kim C, Oh N, Park JH, Hong SW, Kang MS, Mao C, Han DW. 2024. Tailoring photobiomodulation to enhance tissue regeneration. *Biomaterials* **309**:122623.

140. Sezgin B, Tatar S, Karahuseyinoglu S, Sahin GN, Ergun Y, Meric G, Ersoy K. 2021. The effects of oral mucosa-derived heterotopic fibroblasts on cutaneous wound healing. *J Plast Reconstr Aesthet Surg* **74**: 2751–2758.

141. Shen Q, Guo H, Yan Y. 2024. Photobiomodulation for Neurodegenerative Diseases: A Scoping Review. *Int J Mol Sci* **25**: 1625.

142. Shingyochi Y, Kanazawa S, Tajima S, Tanaka R, Mizuno H, Tobita M. 2017. A Low-level carbon dioxide laser promotes fibroblast proliferation and migration through activation of akt, erk, and jnk. *PLoS ONE* **12**: e0168937.

143. Shirasaka, T., Miyagawa, S., Fukushima, S., Kawaguchi, N., Nakatani, S., Daimon, T., Okita, Y., and Sawa, Y. 2016. Skeletal myoblast cell sheet implantation ameliorates both systolic and diastolic cardiac performance in canine dilated cardiomyopathy model. *Transplantation* **100**: 295–302.

144. Smola H, Thiekötter G, Fusenig NE. 1993. Mutual induction of growth factor gene expression by epidermal-dermal cell interaction. *J Cell Biol* **122**: 417–429.

145. Solmaz H, Ulgen Y, Gulsoy M. 2017. Photobiomodulation of wound healing via visible and infrared laser irradiation. *Lasers Med Sci* **32**: 903–910.

146. Sun CC, Chiu HT, Lin YF, Lee KY, Pang JH. 2015. Y-27632, a ROCK Inhibitor, Promoted Limbal Epithelial Cell Proliferation and Corneal Wound Healing. *PLoS One* **10**: e0144571.

147. Sun, J., Qiao, Y. N., Tao, T., Zhao, W., Wei, L. S., Li, Y. Q., Wang, W., Wang, Y., Zhou, Y. W., Zheng, Y. Y., Chen, X., Pan, H. C., Zhang, X. N., and Zhu, M. S. 2020. Distinct roles of smooth muscle and non-muscle myosin light chain-mediated smooth muscle contraction. *Front Physiol* **11**: 593966.

148. Tam SY, Tam VCW, Ramkumar S, Khaw ML, Law HKW, Lee SWY. 2020. Review on the cellular mechanisms of low-level laser therapy use in oncology. *Front Oncol* **10**:1255.

149. Taniguchi D, Dai P, Hojo T, Yamaoka Y, Kubo T, Takamatsu T. 2009. Low-energy laser irradiation promotes synovial fibroblast proliferation by modulating p15 subcellular localization. *Lasers Surg Med* **41**: 232–239.

150. Tao, H., Araki, M., Sato, T., Morino, S., Kawanami, R., Yoshitani, M., and Nakamura, T. 2006. Bronchoscopic treatment of postpneumonectomy bronchopleural fistula with a collagen screw plug. *J Thorac Cardiovasc Surg* **132**: 99–104.

151. Thummarati P, Laiwattanapaisal W, Nitta R, Fukuda M, Hassametto A, Kino-Oka M. 2023. Recent Advances in Cell Sheet Engineering: From Fabrication to Clinical Translation. *Bioengineering (Basel)* **10**:211.

152. Tokunaga, Y., Kita, Y., and Okamoto, T. 2020. Analysis of Risk Factors for Bronchopleural Fistula after Surgical Treatment of Lung Cancer. *Ann Thorac Cardiovasc Surg* **26**: 311–319.

153. Trepat X, Chen Z, Jacobson K. 2012. Cell migration. *Compr Physiol* **2**: 2369-2392.

154. Tsumanuma, Y., Iwata, T., Kinoshita, A., Washio, K., Yoshida, T., Yamada, A., Takagi, R., Yamato, M., Okano, T., and Izumi, Y. 2016. Allogeneic transplantation of periodontal ligament-derived multipotent mesenchymal stromal cell sheets in canine critical-size supra-alveolar periodontal defect model. *BioResearch open access* **5**: 22–36.

155. Ueno, K., Takeuchi, Y., Samura, M., Tanaka, Y., Nakamura, T., Nishimoto, A., Murata, T., Hosoyama, T., and Hamano, K. 2016. Treatment of refractory cutaneous ulcers with mixed

sheets of peripheral blood mononuclear cells and fibroblasts. *Scientific reports* **6**: 28538.

156. Vijayashree RJ, Sivapathasundharam B. 2022. The diverse role of oral fibroblasts in normal and disease. *J Oral Maxillofac Pathol* **26**: 6–13.

157. Watanabe K, Ueno M, Kamiya D, Nishiyama A, Matsumura M, Wataya T, Takahashi JB, Nishikawa S, Nishikawa S, Muguruma K, Sasai Y. 2007. A ROCK inhibitor permits survival of dissociated human embryonic stem cells. *Nat Biotechnol* **25**: 681–686.

158. Wickenheisser VA, Zywot EM, Rabjohns EM, Lee HH, Lawrence DS, Tarrant TK. 2019. Laser Light Therapy in Inflammatory, Musculoskeletal, and Autoimmune Disease. *Curr Allergy Asthma Rep* **19**:37.

159. Wirth A. 2010. Rho kinase and hypertension. *Biochim Biophys Acta* **1802**: 1276–1284.

160. Wood S, Jayaraman V, Huelsmann EJ, Bonish B, Burgad D, Sivaramakrishnan G, Qin S, DiPietro LA, Zloza A, Zhang C, Shafikhani SH. 20104. Pro-inflammatory chemokine CCL2 (MCP-1) promotes healing in diabetic wounds by restoring the macrophage response. *PLoS One* **9**: e91574.

161. Yadav A, Saini V, Arora S. 2010. MCP-1: chemoattractant with a role beyond immunity: a review. *Clin Chim Acta* **411**: 15701579.

162. Yamamoto N, Ueno K, Yanagihara M, Kurazumi H, Tanaka Y, Oga A, Shimokawa M, Harada E, Tanaka T, Hamano K. 2023. Allogenic multilayered fibroblast sheets promote anastomotic site healing in a rat model of esophageal reconstruction. *Am J Transl Res* **15**: 3217–3228.

163. Yanagihara M, Matsuno Y, Ueno K, Kurazumi H, Suzuki R, Tanaka T, Hamano K. 2023. Fibroblasts are the most suitable cell source for regenerative medicine due to their high intracellular fibroblast growth factor 2 content. *Biochem Biophys Rep* **35**: 101510.

164. Yee HF Jr, Melton AC, Tran BN. 2001. RhoA/rho-associated kinase mediates fibroblast contractile force generation. *Biochem Biophys Res Commun* **280**: 1340–1345.

165. Yoshimine S, Ueno K, Murakami J, Saito T, Suzuki R, Asai Y, Ikeda E, Tanaka T, Hamano K. 2022. Autologous multilayered fibroblast sheets can reinforce bronchial stump in a rat model. *Semin Thorac Cardiovasc Surg* **34**: 349–358.

166. Yoshimine, S., Tanaka, T., Murakami, J., Yamamoto, N., Ueno, K., Kurazumi, H., Ikeda, E., & Hamano, K. 2023. Postoperative changes in a bronchial stump following covering with free fat tissue in a rat model. *EJCTS* **63**(5).